# Locations and magnitudes of historical earthquakes in the Sierra of Ecuador (1587-1996)

Céline Beauval, H. Yepes, William Bakun, J. Egred, A. Alvarado, Juan-Carlos Singaucho

# Locations and magnitudes of historical earthquakes in the Sierra of Ecuador (1587-1996)

Céline Beauval, Hugo Yepes, William H. Bakun, José Egred, Alexandra Alvarado, and Juan-Carlos Singaucho

In press in Geophysical Journal International, February 2010

Corresponding author:

Céline Beauval

LGIT

BP 53,

38041 Grenoble Cedex 9

France

Celine.Beauval@obs.ujf-grenoble.fr

**Abstract**

The whole territory of Ecuador is exposed to seismic hazard. Great earthquakes can occur in the subduction zone (e.g. Esmeraldas, 1906, $M_w$ 8.8), whereas lower magnitude but shallower and potentially more destructive earthquakes can occur in the highlands. This study focuses on the historical crustal earthquakes of the Andean Cordillera. Several large cities are located in the Interandean Valley, among them Quito, the capital (~2.5 millions inhabitants). A total population of ~6 millions inhabitants currently live in the highlands, raising the seismic risk. At present, precise instrumental data for the Ecuadorian territory is not available for periods earlier than 1990 (beginning date of the revised instrumental Ecuadorian seismic catalogue); therefore historical data are of utmost importance for assessing seismic hazard. In this study, the Bakun & Wentworth (1997) method is applied in order to determine magnitudes, locations, and associated uncertainties for historical earthquakes of the Sierra over the period 1587-1976. An intensity-magnitude equation is derived from the four most reliable instrumental earthquakes ($M_W$ between 5.3 and 7.1). Intensity data available per historical earthquake vary between 10 (Quito, 1587, Intensity ≥ VI) and 117 (Riobamba, 1797, Intensity ≥ III). The bootstrap resampling technique is coupled to the Bakun & Wentworth method for deriving geographical confidence contours for the intensity centre depending on the dataset of each earthquake, as well as confidence intervals for the magnitude. The extension of the area delineating the intensity centre location at the 67% confidence level ($\pm 1\sigma$) depends on the amount of intensity data, on their internal coherence, on the number of intensity degrees available, and on their spatial distribution. Special attention is dedicated to the few earthquakes described by intensities reaching IX, X and XI degrees. Twenty-five events are studied, and nineteen new epicentral locations are obtained, yielding equivalent moment magnitudes between 5.0 and 7.6. Large earthquakes seem to be related to strike slip faults between the North Andean Block and stable South America to the east, while moderate earthquakes ($M_w \leq 6$) seem to be associated with to thrust faults located on the western internal slopes of the Interandean Valley.

**Keywords**: Intensity data, Historical seismicity, Ecuador

## Introduction

In any region, the essential elements for estimating seismic hazard are seismic catalogues, localization and characterization of active faults (or definition of seismic source zones), and ground-motion prediction models adapted to the region under study (Esteva 1968; McGuire 2008; Beauval & Scotti, 2003, 2004). The present work deals with the first element, the seismic catalogue, which is the basis for characterising potential seismic source zones, especially in a country where a lot of work is still to be done for identifying potential active faults. The Ecuadorian seismic network (RENSIG), maintained by the Geophysical Institute in Quito (IG, part of the Escuela Politecnica Nacional, EPN), provides instrumental locations and magnitudes for the period 1990-present. For earlier periods, international catalogues can provide instrumental solutions for earthquakes with significant magnitude (EHB Centennial catalogue, Engdahl & Villaseñor (2002); USGS/NEIC PDE catalogue or CMT catalogue). However, as will be shown, very few moderate magnitudes have an instrumental characterization. They correspond to shallow but damaging events that occurred before 1976, originating on faults cutting the two Andean ranges in Central Ecuador. Nonetheless, much work has been done over the last 40 years to gather information on Ecuadorian past events and assign MSK intensity to the available observations (CERESIS, 1985; Egred, 2009a, 2009b). This intensity catalogue covers the last 470 years with the earliest events reported dating back to the XVI$^{th}$ century, a few years after the arrival of the Spaniards in Ecuador. Earthquakes are reported if the maximum intensity reached at least the degree V. Based on the intensity distribution in space, isoseismal maps have been drawn for the most significant earthquakes (e.g. Egred 2004), and epicentral locations have been determined based on these isoseismal maps. However, little work has been devoted to magnitude estimation. Until now, magnitude estimates were based solely on maximum intensity and the magnitude-intensity equation of Gutenberg and Richter (1956). Several methods have been proposed in the literature for determining locations and magnitudes of earthquakes, e.g. methods by Gasperini et al. (1999), Musson and Jimenez (2008), Bakun & Wentworth (B&W, 1997 and further publications by Bakun). For the present study, the B&W method is chosen. It makes use of individual intensity observations and uncertainties are quantified in an objective and reproducible way. This method has been applied in many different tectonic contexts using different data sets, and has proved its efficiency as well as its difficulties and limits (e.g. Turkey: Parsons et al. 2004; France: Bakun & Scotti 2006; Germany: Hinzen & Oemisch 2001; Japan: Bakun 2005; Venezuela: Palme et al. 2005). After establishing the intensity attenuation model and checking

the method on the calibration events, magnitude and locations are determined for nineteen historical events located in the Ecuadorian Andes.

## Regional settings and data

The Andes, the major physiographic feature of Western South America, is the result of the subduction of the Pacific oceanic lithosphere beneath the South American plate (e.g. Nieto 1991; Espinosa et al. 1991a). In Ecuador, three N-S trending geologic and geomorphic zones can be distinguished (Fig. 1): (1) the coastal plain to the west (Costa), (2) the central Andean mountainous area, and (3) the eastern lowlands (Oriente) which are part of the upper Amazon basin. This study focuses on the Andean range (also known as "Sierra"), 150 km wide on average, which includes three geologic and geomorphic zones: the Western Cordillera, the Interandean Valley, and the Eastern Cordillera (Cordillera Real). The high Interandean Valley (2,200 to 3,000 m in elevation) is a geomorphic depression not wider than 30 km that is very well developed between the two cordilleras, and filled with Quaternary volcanoclastic and pyroclastic deposits north of latitude 1.7º S. South of 1.7º S, spacious intra-mountainous basins show sedimentary fillings lacking the fresh volcanic deposits of the Interandean Valley due to the absence of Quaternary volcanic activity. Almost half of the Ecuadorian population resides in the Sierra.

The B&W (1997) method requires an intensity attenuation model, which is best obtained from calibration events with both a reliable instrumental and a macroseismic determination. Analysing the intensity catalogue (Egred, 2009a, 2009b) with respect to the instrumental EPN catalogue, few events appear to meet this criteria in the Sierra. Three instrumental events described by a large set of intensities will be used (Table 1): Pujili (1996, $M_W$ 5.9), Pomasqui (1990, $M_W$ 5.3), and Salado-Reventador (1987, $M_W$ 7.1). A fourth event with magnitude and location available in the EHB Centennial catalogue is included in the calibration: the Pastocalle event (1976, $M_b$ 5.7). Unfortunately, there is no moment magnitude available for this earthquake. A few other Sierra events were analysed for calibration purposes (Santa Rosa, $M_W$ 5.1, 2000/10/8; Vacas Galindo, $M_b$ 5.3, 1994/5/11), but their intensity distributions relative to epicentral distances display curious trends, probably due to incompleteness of observations in space for lower intensities (III and IV). Furthermore, the Tena earthquake (1987, $M_W$ 6.4) has an EHB solution close to the ISC solution; however the intensity distribution versus epicentral

distance relation is counter-intuitive, for highest intensity degrees the median distances are increasing with increasing intensity degrees (from intensity V to VII). This may be due to a strong site effect in the Interandean Valley south-west of the epicentre, or to a directivity effect of the seismic waves related to the fault mechanism. We decided to discard these events and to establish the intensity-magnitude equation on few, but reliable, events. Ideally, the intensity-magnitude equation should be established with a first set of earthquakes, and then the B&W method should be applied on another reliable and independent set of instrumental earthquakes (e.g. Bakun & Hopper, 2004). Obviously such a validation of the equation is not possible here. Nevertheless, three events with an EHB determination (Engdahl et al. 1998; Engdahl & Villaseñor 2002) can be partially used as test events (Table 1): Pelileo (1949), Due-Reventador (1955), Pepinales (1961). The method is then applied to all earthquakes reported in the intensity catalogue (Egred, 2009b) with a minimum of 10 intensity observations. The study covers an area approximately 300km-long and 80 km-wide, the two mountain ranges of the Ecuadorian Andes and the Interandean Valley.

## Methodology

### *Establishing the attenuation model from calibrating events*

Intensity, like seismic energy, attenuates with increasing distance from the epicentre. The calibrating earthquakes provide a set of intensity degree / median distance couples that are used to linearly solve the following system (e.g. Bakun, 2006):

$$I = a + bM_w + cLog\sqrt{(R^2 + h^2)} + d\sqrt{(R^2 + h^2)} \qquad \text{(Eq. 1)}$$

where $M_W$ is the moment magnitude, R the epicentral distance, h a generic depth, and a, b, c, d, the coefficients to be determined. Each earthquake provides a set of intensity degrees and associated median hypocentral distances (Fig. 2; Table 2). Not all low intensity levels (III, IV) are included; those shown to be incomplete in space are discarded. As the coefficient d we obtained is close to zero and has an associated uncertainty larger than its value, the linear dependence of intensity with hypocentral distance is abandoned and the system is solved for three parameters only (a, b, c). The final attenuation model takes into account moment magnitude and geometrical spreading:

$$I = -(0.85 \pm 0.76) + (2.41 \pm 0.14)M_W - (5.39 \pm 0.35)\log \Delta_h \qquad \text{(Eq. 2)}$$

where I is the intensity, $\Delta_h$ is the slant distance. The depth of the instrumental events bears rather large uncertainties, therefore a fixed 10-km depth is used here for all crustal events. Uncertainty on the coefficient a is quite large, as found by other authors (e.g. Bakun, 2005); there is also a trade-off between coefficients a and b. The attenuation model is superimposed to the intensity data versus distance (Fig. 2); the model is consistent with the assigned intensity values and median distances. This attenuation model is only valid for crustal earthquakes occurring within the Sierra, and preferably with magnitudes $M_W$ between 5.3 and 7.1 (range of magnitude of calibration events). This model predicts higher attenuation with distance than models established in stable continental regions (e.g. Atkinson & Wald 2007), which is expected in a region that is geologically younger and dotted with volcanoes (e.g. Azzaro et al. 2006). Interestingly, Egred (2004) noted that for several large earthquakes, isoseismals are elongated in the north-south direction, which could indicate a lower attenuation of seismic waves along the axis of the Interandean Valley than in the east-west direction perpendicular to the mountain chains. Unfortunately, it is not possible to take into account differences in attenuation according to azimuth due to the few available calibrating events. Furthermore, note that directivity and extended sources are not represented in this simple point-source model. If using Equation 2 in the future for predicting intensities produced by a given magnitude earthquake in the Sierra, one cannot expect to correctly predict intensities at very close distance to the epicentre for earthquakes of magnitude higher than ~6.5. Applying the intensity-magnitude equation for large earthquakes will require imposing saturation of the intensity at a given distance from the epicentre (e.g. at a distance equivalent to half of the fault length, applying Wells & Coppersmith, 1994, magnitude-fault length equations).

### *Determination of magnitude and location from intensities*

Following the B&W methodology, a grid is defined over the felt region including all intensity observations describing the studied event, with a grid step of 2.5 to 5 km depending on the desired precision. Each grid node is a potential location for the source. At each node, the intensity magnitude $M_I$ and the associated root mean square rms[$M_I$] are calculated. The intensity magnitude $M_I$ is calibrated to equal moment magnitude $M_W$. Intensity magnitude is

simply the mean value of all magnitude values inferred from the individual intensity assignments:

$$M_I = \frac{1}{n}\sum_n M_i \qquad \text{(Eq. 3)}$$

where $M_i=[I_i+0.85+5.39\log\Delta_i]/2.41$, $I_i$ is the MSK intensity value at site i, $\Delta_i$ is the slant distance (in km) of observation i from the assumed grid point, and n the number of intensity assignments. Iso-contours of magnitude estimates can then be plotted.

The rms quantifies the error between observed and estimated intensities:

$$rms[M_I] = rms[M_I - M_i] - rms_0[M_I - M_i], \qquad \text{(Eq. 4)}$$

with $rms[M_I - M_i] = \{\sum[W_i*( M_I - M_i)]^2/\sum W_i^2\}^{1/2}$ and $rms_0[M_I - M_i]$ the minimum $rms[M_I - M_i]$ over the grid of assumed trial source locations, and $W_i$ the following weighting function (B&W 1997):

$$W_i = \begin{cases} 0.1 + \cos[(\Delta_i/150)*\pi/2], & \text{for } \Delta_i \le 150 \text{ km}, \\ 0.1, & \text{for } \Delta_i > 150 \text{ km}. \end{cases} \qquad \text{(Eq. 5)}$$

Observations located close to the assumed epicentre are therefore given a higher weight than observations at large distances. However, note that in general tests on Ecuadorian earthquakes showed that results are similar with or without using the weighting function (very few exceptions, as discussed later in the paper). The node corresponding to the minimum $rms[M_I]$ is the intensity centre (IC); it is the point source where the error between observed and estimated intensities is lowest. The magnitudes at trial source locations within the confidence-level contour of interest (67%) constitute the uncertainty distribution for the intensity magnitude of the earthquake (Bakun, 1999). The intensity centre corresponds to the location on the fault plane where the energy release is highest (i.e. to the location of maximum fault displacement, or moment centroid); therefore the intensity centre does not always match the epicentre (Bakun 2006). Unfortunately, the moment centroid is not available for the calibrating events. In any case, if some candidate causative fault is located within the confidence contours, the earthquake epicentre might be preferably localized on the fault. This "preferred" location might be different from the location of the intensity centre corresponding to the minimum rms.

Few historical earthquakes in the Sierra are described by intensity observations higher than IX (Table 4). Exceptions include the Pelileo earthquake (1949/8/5) with maximum intensities reaching X, and the Riobamba event (1797/2/4) with highest intensities of XI. Intensities higher than VIII in remote times have a high probability of being over-estimated. The adobe houses of these periods are destroyed or damaged beyond repair for intensity levels of VII-VIII, thus discrimination between levels VIII, IX, X and XI is really difficult (Ambraseys 2001; Ambraseys & Bilham 2003; Parsons et al. 2004). For these two Sierra events, location and magnitude are calculated taking into account intensities up to level VIII, then up to levels IX, X (and XI for Riobamba), in order to evaluate the influence on the results of highest intensity levels. Note that, unlike most intensity catalogues (e.g. the French catalogue, see Bakun & Scotti, 2006), no information on the quality of the individual intensity observations is provided in the Ecuadorian catalogue. However, as will be shown later, testing the application of the method using different datasets extracted from the original dataset gives indications of the stability of the results.

Site effects can influence intensity observations (e.g. Pasolini et al., 2008), and thus bias magnitude and intensity centre location estimates. While establishing the attenuation model, the influence of site effects is reduced by calculating median distances after eliminating outliers (observations higher or lower than mean±2$\sigma$). Nonetheless, Bakun & Wentworth (1997) proposed a method to take site effects into account through the calculation of site correction factors based on the calibrating events. To calculate such amplification factors, several observations must be available at a given site (B&W 1997). Relying only on four calibrating events prevents us from calculating reliable and meaningful correction factors. In this investigation site effects will not be taken into account. However, as already said, tests will be performed to check the influence of potentially over-estimated higher intensity degrees.

### *Determining confidence contours applying systematically bootstrap resampling*

The intensity centre location corresponds to the node of the grid with highest probability, however other nodes of the grid have non-zero probability of being the intensity centre. Therefore, it is of importance to identify all potential locations together with the associated probability, in other words to define the confidence contours that delineate the areas containing given probability levels that the intensity centre lays within the contours. At first,

the tables associating contours of rms values to different levels of confidence depending on the number of intensity assigned values, as published by Bakun & Wentworth (1999), were applied directly (results not shown in the paper). However results for the Sierra events showed that the location uncertainty resulting from a boostrap resampling (Efron, 1982) is always smaller than inferred from the appropriate California contours with similar numbers of intensity observations (as also found in France by Bakun & Scotti, 2006). Therefore, the bootstrap statistical technique is coupled to the B&W (1997) method to determine confidence contours adapted to each earthquake (see e.g. Bakun, 2006). The complete calculation is performed 1000 times, each time the intensity data set is resampled (random sampling with replacement, keeping the size of the original dataset constant), and 1000 intensity centres are obtained together with 1000 intensity magnitude estimates. The results show that the spatial distribution of bootstrapped intensity centres always mimics the rms contours. Therefore, the 50% confidence contour is the rms iso-contour containing 500 of these intensity centres, the 67% contour is the rms iso-contours containing 670 of these intensity centres, and so on. The uncertainty based on bootstrap resampling can be considered as the uncertainty due to the use of only a sample of the population, assuming that the model is perfect. This should not be confused with the true epistemic uncertainty on the epicentre, which is not obtainable by any statistical means.

### *Application to the calibration events*

The minimum requirement for the validation of the method is to obtain satisfactory results for the calibrating events. Location and magnitude estimates derived from the application of the B&W (1997) method on the four instrumental events are reported in Table 3 and results are displayed in Figures 4 to 5. Note that the calculations were performed with and without the weighting function, and the results were similar. From now on, results are displayed for calculations with weights. The intensity centres and intensity magnitudes obtained are consistent with the instrumental estimations. There is little difference in magnitudes estimated for locations at the hypocentre or at the intensity centre.

*Pujili (1996, $M_W$ 5.9, Figs. 4a and 5a).* This earthquake occurred in Cotopaxi province and affected mostly Pujili county, where the strongest damage was reported (many adobe houses partially collapsed; light damage in brick houses). Intensity observations are numerous, 87

between III and VII, and rather evenly distributed in space. As shown in Figure 4a, the intensity centre location is 8km to the southwest of the instrumental epicentre, consistent with the hypothesis that the earthquake occurred on a N-S fault dipping to the west (La Victoria fault, Lavenu et al. 1995). Confidence contours corresponding to 50, 67 and 95% are narrow (5km×5km for 67%). The intensity magnitude at the instrumental epicentre is 5.85, and 5.97 at the intensity centre (5.9-6.01 at the 67% confidence level). Individual magnitudes inferred from all intensity observations higher than III are plotted versus slant distance. No bias is observed related to intensity degree: the trends corresponding to the different intensity degrees overlap as expected (see e.g. Bakun & Scotti, 2006). A moving average mean for the intensity magnitude is calculated (every 10km). Its value is more or less stable with distance (which means no bias, Fig. 5a).

*Pomasqui (1990, $M_W$ 5.3, Figs. 4b and 5b).* The earthquake occurred on one of the two northern segments that are part of the Quito thrust fault system (north-south trend), the San Juan de Calderon and Catequilla segments (Alvarado 2009). The intensity dataset is made of 66 observations between IV and VI, distributed in a north-south direction following the main road. The intensity centre is located 7km to the north of the epicentre, at the end of the Catequilla fault segment. The confidence contour 67% covers an area of approximately 10km×5km. The confidence contour at 95% is elongated in the NW-SE direction, as there is no intensity data in this direction. Magnitude at the epicentre is 5.28 and 5.4 at the intensity centre (5.3-5.6 at the 67% confidence level). The moving mean average for the intensity magnitude is stable over distance (no bias with distance, Fig. 5b).

*Salado-Reventador (1987, $M_W$ 7.1, Figs. 4c and 5c).* The earthquake occurred on the border between Napo and Sucumbíos provinces, where highest damages were reported in buildings and natural settings. Other provinces were also heavily affected (Imbabura, Pichincha and east Carchi). The catastrophic debris flow triggered by this earthquake caused an estimated death toll of more than one thousand people and severe destruction of the Trans-Ecuador oil pipeline. The estimated economic loss reached about one billion U.S. dollars (Kawakatsu & Proaño, 1991). An extensive intensity collection survey was led (228 ≥ III, Espinosa et al. 1991b; Egred, 2009b). Intensity observations of IV are reported for distances up to 200 km. As shown in Figure 4c, the instrumental epicentre location is right on the potential causative thrust fault (Salado, see Soulas et al. 2001), with a probable extension on a fault segment to the north (Reventador segment, Soulas et al. 2001). The intensity centre is located 4 km away from the

instrumental epicentre, which is located in between confidence contours 50 and 67%. The 67% confidence contour delineates an area of approximately 6km×6km. Equivalent moment magnitude is 7.0 at the intensity centre, and 6.96 at the instrumental epicentre (Table 3). The moving average mean for the intensity magnitude is very stable over distance (Fig. 5c).

*Pastocalle (1976, $M_b$ 5.7, Figs. 4d and 5d).* This earthquake caused heavy damage in rural villages of Cotopaxi province (mainly adobe houses). The location of the causative fault is not obvious. The instrumental epicentre and the intensity centre are ~6km apart. The instrumental location is located on the 67% confidence contour. Taking into account the 95% confidence area and up to a ~10 km uncertainty on the instrumental epicentre, a location along a northwestern branch of the inverse Saquisili-Poalo-Yambo fault system (Toacazo segment: Alvarado, 2009) is conceivable. The mean average magnitude is very stable with distance (Fig. 5d). The equivalent moment magnitude obtained (5.89 at intensity centre, 5.8 at epicentre) is slightly higher than the instrumental magnitude, which is possible if the $M_b$ 5.7 magnitude was slightly saturated.

### *Application on three instrumental events*

Three events can be partially used as test events, i.e. earthquakes that have instrumental determination and that do not take part in the calibration. These events are the Pelileo (1949, G-R $M_S$ 6.8), Due-Reventador (1955, UK M 6.8), and Pepinales (1961) earthquakes. These events can be used only partially as test events, because the magnitudes are not moment magnitudes (no magnitude estimate for Pepinales) and instrumental locations bear uncertainties much higher than the calibrating events localised by the EPN. However, it is worth testing the application of the method on these events which have partial instrumental determinations.

*Pelileo (1949, M 6.8, Fig. 6)*. This earthquake was highly destructive in the Tungurahua and Cotopaxi provinces, and partially destructive in the Chimborazo and Bolívar provinces. In the epicentral zone, the Pelileo and Patate villages were destroyed, whereas most houses in Guano and Ambato collapsed (Ramirez, 1951). Approximately 6,000 deaths were reported. Intensities as high as X were assigned but these intensities are potentially over-estimated and must be considered with caution. In Pelileo and its surroundings, the soil is apparently prone to site effects (Woodward-Clyde 1981), and furthermore, large landslides increased damages and

casualties. Note that there is an EHB solution for this event (coordinates (-1.5; -78.25); Engdahl & Villaseñor, 2002), but it is located more than 40 km to the south-east from the highest intensities and cannot be considered reliable. At first, calculations are performed based on intensity observations up to IX (Fig. 6a). The intensity centre is located close to the epicentre determined from isoseismals (Egred, 2009b) and is well constrained (area of the 67% contour: 10km×8km). Nonetheless, the instrumental location that is currently considered the most reliable (Woodward-Clyde 1981) is located 20 km to the northeast, within the 95% confidence contour. The equivalent moment magnitude is 6.3 at the intensity centre, and close to 6.6 at the instrumental epicentre. Taking into account a probable 0.2 unit uncertainty on the G-R magnitude estimate (Bakun, 1999), these results can still be considered consistent with a G-R 6.8 magnitude. The fault should extend a minimum of 20 km (M6.3, Wells and Coppersmith, 1994). According to the report by Woodward-Clyde (1981), the causative fault might be a SW-NE fault segment north of the instrumental epicentre (Pucara segment, Alvarado 2009). Considering both the instrumental and the intensity centre locations, the earthquake might have occurred on a SW-NE fault system made of the north-eastern prolongation of the Pallatanga fault system (which is very well identified to the south-west) joined with the Mundug and the Pucara faults. The intensity centre would then be located very close to the causative fault plane.

Several sensitivity tests were performed. Previous results are based on intensities up to degree IX. When intensities X, assigned at Pelileo and at locations within a 5km-radius from this town are included, calculations yield an identical epicentral location but the confidence contours enclose narrower areas (Fig. 6b). Woodward-Clyde et al. (1981) justified the high intensity reported at Pelileo arguing the existence of site effects. To eliminate the influence of potentially over-estimated IX intensity assignments, the calculations were performed taking into account intensities up to VIII (Fig. 6c given as an electronic supplement). The 67% and 95% areas are extended, but the intensity centre remains identical and the associated magnitude is slightly lower (6.5 instead of 6.6 at the instrumental epicentre). Furthermore, as Singaucho (2009) provides a revision of intensity assignments for this earthquake, the calculations were performed based on the re-visited 58 intensities (III to X) instead of the 82 original observations. Intensity observations are reduced because it was not possible to have access to all original documents; however the intensity centre location is still unchanged. Only future work, based on other kind of data (waveforms, neotectonics) will enable confirmation of the

SW-NE orientation of the causative fault. However, in the zone of highest destruction (Patate and Pelileo villages) where the intensity centre is located, landslides triggered by the earthquake covered a large area, making it difficult to presently identify evidence of surface rupture.

*Due-Reventador (1955, UK PAS magnitude 6.8, Fig.* 7a*).* The intensity distribution does not enable us to localise the intensity centre with confidence, probably because the epicentre is far from the observation "network" (35-40 km). Therefore, only the intensity magnitude will be compared to the magnitude at the EHB instrumental location (Engdahl & Villaseñor, 2002). Note that although the intensity centre is not well constrained, it is located close to the instrumental epicentre. Equivalent magnitude at the epicentre is 7.0, which is compatible with a UK magnitude 6.8 that might bear a 0.2 uncertainty. Taking into account a possible 15km uncertainty on the instrumental epicentre, the equivalent moment magnitude predicted by the intensity dataset at these locations ranges from 6.8 to 7.2.

*Pepinales (1961, Fig.* 7b*).* This earthquake was felt throughout the whole country, and produced extensive damage in the southern areas of Chimborazo province (collapsing of adobe constructions). There is an EHB instrumental location (Engdhal & Villaseñor, 2002) that might bear some error (15km-uncertainty is assumed in Fig. 8b). The intensity centre obtained lies close to the instrumental epicentre (10 km), which is located on the 50% and 67% confidence contours, to the north of Alausi town. Both the intensity centre and the instrumental epicentre are within the Pallatanga SW-NE strike-slip system (Winter 1990, Alvarado 2009). Equivalent moment magnitude at the intensity centre is 6.5 (6.3 at instrumental epicentre), and the 67% confidence interval is 6.3-6.8. However note that the confidence contours also allow possible locations of the intensity centre south-east of Alausi. Moreover, the valley where the Pallatanga fault system lies, that would be the epicentral region according to the 67% confidence contour, does not display high intensities (VII and VIII). This lack of high intensity observations is surprising, as this valley was already well populated at the time. Therefore, the actual data available do not enable us to provide a satisfactory solution for this earthquake. The Guamote-Huigra fault system (Alvarado, 2009) lies in the valley where the nest of intensities VII and VIII is located. This could also be a potential candidate for this earthquake, yielding a lower magnitude (6.1-6.2). More work is required to clearly identify the responsible fault segment.

## Determination of location and magnitude of historical events

The method is applied to historical events for which no instrumental determination is available (Table 4). All events with a minimum of 10 intensity observations higher or equal to III were considered, which results in more than 20 studied earthquakes. However locations cannot be obtained for all of them. Some events are described by a large intensity dataset well distributed in space (various distances and azimuths), others are described by only 2 intensity degrees with unevenly distributed observations. When intensities reported are few or when the probable epicentre is far outside the "network" of observations, locating the intensity centre is not possible. This is the case for the three events that occurred north of the Colombian border (1843, 1923, 1953). As these events are described both by intensities collected in Ecuador and in Colombia, the analysis of these earthquakes is left for future collaborative work between both countries. Bakun & Wentworth (1997) demonstrated that their method is particularly adapted to Californian historical earthquakes with very few observations (down to 5). This might be less true for earthquakes in the Sierra of Ecuador, as even for recent earthquakes the absence of observations in the mountain ranges to the east and to the west of the populated Interandean Valley represents a difficulty. In the following, $M_{IC}$ is the intensity magnitude estimated at the intensity centre, equivalent to a moment magnitude. For all earthquakes, the uncertainty on magnitude, i.e. 67% probability intervals deduced from the magnitudes of the bootstrap intensity centres lying within the 67% spatial confidence contour, are also reported (Table 5). $M_{Preferred}$ is the magnitude obtained at a "preferred" location for the epicentre, different from the intensity centre (the minimum rms location) but located within the confidence contours.

### *Earthquakes of the second half of the XX$^{th}$ century*

The earthquakes studied are Aloasi (1976, $I_{max\_obs}$ VII, $M_{IC}$=5.), Cusubamba (1962, $I_{max\_obs}$ VII, $M_{preferred}$=5.8-6.0), Pasa (1960, $I_{max\_obs}$ VII, $M_{Preferred}$=5.6-5.7), Latacunga (1958, $I_{max\_obs}$ VI, $M_{IC}$=5.0), and Atahualpa (1955, $I_{max\_obs}$ VIII, $M_{IC}$=6.14). Magnitudes obtained for these earthquakes of the second half of the XX$^{th}$ century are moderate (5-6), as expected, since these earthquakes are not reported in the international seismic catalogues.

The magnitude 5.0 Aloasi earthquake was felt in a narrow rural area between Pichincha and Cotopaxi provinces, its confidence contours are indeed narrow (67%, 5km×5km, Fig. 7c given

as electronic supplement). This earthquake might be related to the Pastocalle earthquake that occurred less than 2 months earlier 20km to the south. The causative fault might be the northern continuation of La Victoria Fault (Lavenu et al, 1995) or the Machachi SW-NE fault (Soulas et al, 1991).

The Cusubamba earthquake (Fig. 8a) was strongly felt in the central region of Ecuador. The intensity centre falls in a zone where no fault has previously been identified, the 50 and 67% confidence contours delineate quite large zones (only 11 intensity assignments, III to VII) and indicate an intensity centre on the western slope of the Interandean Valley. The 95% contour extends in the direction corresponding to a lack of data, perpendicular to the valley, including the western and eastern slopes. This earthquake might have occurred on the north-south thrust fault system, preferably on the Western slope of the valley, which represents the southern continuation of La Victoria Fault (Lavenu et al, 1995).

The Pasa event (Fig. 8b) also occurred within the Western Cordillera and might be related to the same fault system as the Cusubamba event. The intensity centre, corresponding to the minimum rms, is located within the Western Cordillera where no fault has been identified. The preferred location for the epicentre is close to the 67% confidence contour, on the western slope of the Valley, slightly south of the 1962 event.

The Latacunga earthquake is a small event probably generated by the north-south Alaquez fault (Alvarado 2009); the intensity centre is located on the southern end of this fault (Fig. 8c given as electronic supplement).

Finally, the Atahualpa event (Fig. 9a) was strongly felt in the Imbabura province, but also in the neighbouring Pichincha and Carchi provinces. Many rural adobe buildings collapsed in the epicentral area, and several large landslides cut main roads in Imbabura. This event is well described by 45 assigned intensity points from degree III to VII quite homogeneously distributed. The magnitude is 6.14 at the intensity centre, and 6.1-6.2 at the 67% confidence level. Taking into account the extension of the 95% contour (≈ 30km × 15km), several SW-NE fault segments might be considered as candidate: from west to east, the Apuela segment, the northern segment of the Nanegalito fault system, the northern segment of the Huayrapungo fault segment, or the Otavalo fault (Eguez et al. 2003).

*Earthquakes of the first half of the XX$^{th}$ century*

Earthquakes studied are Toacazo (1944, $I_{max\_obs}$ VII, $M_{Preferred}$=5.6-5.7), Sangolqui (1938, $I_{max\_obs}$ VII-VIII, $M_{IC}$=5.8), Murco (1929, $I_{max\_obs}$ VII-VIII, $M_{IC}$=5.88), Antisana (1914, $I_{max\_obs}$ VIII, $M_{IC}$=6.44), Cajabamba (1911, $I_{max\_obs}$ VII-VIII, $M_{Preferred}$=6.1-6.3).

The Toacazo earthquake (Fig. 9b) produced extensive destruction in rural areas and in the towns of Toacazo and Pastocalle. Fifty and 67% confidence contours delineate quite large zones (25km×10km for 50%). The intensity centre is located within the Western Cordillera, on geologic folds that are not considered as seismically active (Alvarado 2009). The preferred location for the epicentre is slightly shifted to the east on the 50% confidence contour, on the slope of the Interandean valley. The sources of the Pastocalle (1976) and Toacazo events might be the same: a segment on a northwestern branch of the inverse Saquisili-Poalo-Yambo fault system (Alvarado, 2009). Note that there is an instrumental location for this earthquake (-0.5, -79.0) from CGS, but it is very likely that it bears an error of at least 30 or 40km.

The Sangolqui earthquake (Fig. 10a) was strongly felt in a rather narrow area in a valley south-east of Quito (Los Chillos), many adobe houses collapsed. The 50 and 67% confidence contours point at the Pintag NW-SE fault as the causative fault (Alvarado, 2009). This fault is part of the lineament described by Hall & Wood (1985). The segment can accommodate a magnitude 5.8 earthquake (~9-10km rupture length, Wells & Coppersmith 1994).

The Murco earthquake (Fig. 10b) destroyed the village of Murco and was partially destructive in some other villages in southern areas of Pichincha province. Confidence contours 50, 67 and 95% are rather narrow, delineating a zone where no potentially active faulting has been reported. This earthquake might have occurred on a segment south of the Quito fault system that would be located within the 67 or 95% confidence contours to the west of the intensity centre. Another option would be on the northeastern continuation of the Machachi fault (Soulas et al, 1991). This option is preferred since damages are localized in that direction.

The Antisana event ($M_{IC}$ 6.44, Fig. 11a) was felt over a large region, from Cuenca to the south (Fig. 1) up to Ibarra to the north, with strongest damage in Pichincha province. It triggered several landslides on the slopes of Antisana volcano and surrounding hills. Several reported VIII intensities correspond to landslides and liquefaction effects. The intensity centre is quite well constrained, with rather narrow confidence contours; however within the 95% contour no previous evidence of active faulting has been reported. As the historical documents for this

event have been revised with reassessment of the intensity values and checking of the locations (Singaucho, 2009), this earthquake is an opportunity for evaluating the impact on the estimations of potential "errors" in the data. Some errors in locations were detected, some high intensities based on landslides/liquefaction were eliminated. Recent results have indeed shown that effects such as liquefaction can be poor indicators of overall shaking levels (e.g. Ambraseys & Douglas, 2004). From the original 45 locations of observations, 34 remained (III to VII). The resulting intensity centre and confidence contours remain very stable; only the equivalent moment magnitude slightly decreased from 6.56 to 6.44. Note that the Antisana lineament identified by Hall & Wood (1985) crosses the zone of high damage (intensities VII), 10 km to the north-east of the intensity centre; a fault segment belonging to this lineament could be a possible candidate for this earthquake. More fieldwork is required in this area to determine the causative fault.

The Cajabamba event (Fig. 11b) was strongly felt and produced heavy damage in several sectors of Chimborazo province. The intensity centre and 50/67% contours clearly identify one segment of the SW-NE Pallatanga strike-slip fault system as the source of the earthquake [Eguez et al., 2003, Alvarado, 2009]. By shifting the intensity centre on the same fault segment to the northeast, to the 95% confidence contour, the magnitude deduced from intensities decreases to 6.2. This location of the intensity centre is more in accordance with the lack of intensity observations in the Pallatanga valley to the southwest, a valley that was already well populated at the time.

*Large earthquakes of the XVI-XVIII$^{th}$ centuries*

*Quito (1859/3/22)*

This earthquake (Fig. 12a) produced destruction in a large area; the Cotopaxi, Pichincha and Imbabura provinces, were equally struck (intensities VII). It was felt as far as Guayaquil on the coast (intensity IV ~300km far from Quito, see Fig. 1). Analysing the pattern of the intensity distribution, mainly one intensity degree (VII, see Table 4) extending in a direction north-south over 150km, one anticipates that the B&W method will not be able to localize a reliable intensity centre. Indeed, only a loose 50% confidence contour can be plotted, indicating possible locations to the west and to the east of the intensity observations (figure not shown). One explanation is that this event is not crustal, but is a deep event within the subducting slab

beneath the Andean Range. This would explain the large extension of the VII macroseismic area. Interestingly, this event is one exception regarding the influence of the weighting function on the location and magnitude estimates. If applying the method without the weighting function (all intensity assignments have equal weight whatever the distance to the assumed epicentre is), a different result is obtained (Fig. 12a): the intensity centre can be localised more reliably 15km to the west of Quito. The intensity magnitude at intensity centre is 7.2, however this magnitude estimate cannot be considered reliable if the event is located in the slab as the attenuation model has been derived from crustal shallow earthquakes. As doubt remains, this event is kept in the crustal event list. More work is required to reliably identify its source.

*El Angel (1868/8/15)*

The El Angel earthquake (Fig. 12b) occurred 10 hours before the larger Ibarra event described below. It was strongly felt all over the Carchi province, causing damage to many houses and churches, and dozens of casualties. The damage increased with the following larger Ibarra event (40-50 km to the south), which implies that the magnitude based on the intensity dataset might be overestimated. Essentially two intensity degrees are described (VII and VIII); however the intensity centre and the confidence contours 50 and 67% clearly identify three potential faults within the El Angel fault system (Eguez et al. 2003), all oriented SW-NE: Mira, Tufiño and El Angel (Alvarado 2009). The equivalent moment magnitude obtained at the intensity centre is 6.6, and the 67% probability interval 6.4-6.8. It is likely that damage of the first event cannot be easily separated from damages of the second larger event and this magnitude estimate should be considered with caution.

*Ibarra (1868/8/16)*

The Ibarra earthquake (Fig. 13) is the most destructive earthquake to strike northern Andean Ecuador during historical times. Several cities, namely Atuntaqui, Cotacachi, Ibarra, and Otavalo, were completely ruined, as well as many villages in their neighbourhood. Damages were also reported in churches and houses in Quito. In the Imbabura province, large landslides destroyed roads and haciendas. Several strong aftershocks were reported. Seventy-five intensity assignments ranging from III to IX are available for analysing this event, yielding a 7.27 equivalent moment magnitude at the intensity centre (Fig. 13a, 67% confidence interval: 7.1-7.7). Note that this magnitude is higher than the maximum magnitude of the calibrating events (7.1). The distribution pattern of the intensities, with decreasing values from west (IX

and VIII) to east (VI and V) parallel to the SW-NE trending fault system, favours a location of the intensity centre to the west. Wells and Coppersmith's (1994) generic equation predicts approximately a 70 km rupture for a M 7.27 earthquake. Fault segments within the 95% confidence contour include the Apuela fault to the west, and northern segment of the Huayrapungo fault (Eguez et al. 2003). The next SW-NE trending fault to the east is the Otavalo fault (Eguez et al. 2003). Assuming that the earthquake was generated on the Otavalo fault, the intensity observations would yield a $M_I$ 7.0 event (rupture length ~50 km). Furthermore, a new analysis of the intensity dataset by Singaucho (2009) showed that some intensities reported are rather unreliable. These observations were eliminated in the revised dataset. Unfortunately, Singaucho (2009) could not locate all original documents, and his work provides a set of 31 revised and reliable intensity values, free of geographical location errors and of intensities relying on effects in nature. The new intensity dataset does not include any intensity assignment west or close to the Apuela and Huayrapungo segments (Fig. 13b). Maximum intensity now reaches degree X. The results remain stable (location of intensity centre and associated magnitude), however the confidence contours are extended in the NW-SE direction, with contours 95% and 67% crossing the Otavalo fault. Only future work based on other type of data (tectonic, geology fieldwork) will enable confirmation or rejection of these findings.

*Riobamba (1797/2/4)*

The earthquake that razed Riobamba Antiguo to the ground is the most destructive earthquake in the written history of Ecuador (five centuries), causing at least 25,000 casualties (Egred, 2000, 2004). The city of Riobamba was re-located after the tragedy. Many towns and villages were demolished in the provinces of Chimborazo, Tungurahua and Cotopaxi, but also in some parts of Pichincha and Bolívar. Many large cracks resulted in the topography and many liquefaction effects were observed. The earthquake triggered extensive landslides, covering entire districts of Riobamba city but also creating dams in rivers 50 km to the north. This earthquake was followed by months of aftershocks, some of them increased the destruction. The available intensity dataset is large (Table 4) with 117 intensity values ranging from degree III to degrees X (at 37 locations) and XI (at 3 locations). Intensities X extend over approximately 100km in a north-south direction (Fig. 14). The earthquake was felt in northern Peru (Piura, intensity III, ~400km south of Riobamba). Taking into account all intensities up to IX results in an intensity centre located close to the city of Guano, and yields a 7.6 equivalent moment magnitude (7.5-7.9 at the 67% confidence level, Fig. 14a). The 67% confidence area oriented

NW-SE and extending over approximately 50km is less constrained to the south-east as no intensity observation is available in that azimuth. Taking into account intensities X and XI yields results consistent with the previous one; however the confidence contours are much narrower (Fig. 14b). The weighting function is not taken into account in this case, in order not to give too much weight to observations that might be very close to the fault plane and for which the point source model is not adequate. Using only intensities up to VIII still yields comparable locations of the intensity centre (Fig. 14c given as electronic supplement) as well as applying the method on the revised intensity dataset provided by Singaucho (2009). A magnitude 7.6 earthquake can rupture over ~110 km (Wells & Coppersmith, 1994). The only known fault system able to generate a magnitude 7.6 earthquake in the area is the SW-NE Pallatanga system (Winter, 1990). The most probable fault plane for the Riobamba earthquake is therefore a segment of the Pallatanga fault system that ruptured to the north-east to join the Pucara fault segment (Alvarado, 2009; the Pucara fault segment has been identified as the potential source of the 1949 Pelileo earthquake). The intensity centre would then be located somewhere in the middle of the fault plane. Directivity effects could explain the high intensity observations within the Interandean Valley, and the rather low intensities reported on the southwestern segment of the Pallatanga fault system (VII). More neotectonic fieldwork is required in this area to clearly identify the potential fault segments involved, although this task might be difficult as the recurrent activity of the active volcanoes in the area might have obscured superficial evidence.

Note that the point source hypothesis, which is the basis of the B&W (1997) method and the inherent hypothesis for using an intensity-magnitude relationship considering hypocentral distances, is obviously not fulfilled in this case. B&W have applied this method for earthquakes up to M7.8 (Bakun & Hopper, 2004), using observations located at long distances from the source. For large extended sources, assuming that the energy comes from a point source might lead to an over-estimation of intensity magnitude if using many intensity observations close to the rupture surface (Bakun, 1999). We cannot ignore this fact, however we believe that in the case of the Riobamba event, using only intensities up to VIII and then up to IX reduces this effect. Far enough from the fault, rupture distances between an intensity observation site and any point along the rupture are quite similar. To correctly treat this problem, we would need to establish an intensity-magnitude equation with the nearest distance to the rupture plane (e.g. Ambraseys 2002), which is currently not possible considering the available calibrating events. In the near future, other methods relying on the individual intensity observations for

estimating magnitude and location should be tested on the Riobamba intensity dataset. For example, it will be interesting to test the method by Gasperini et al. (1999), which is intended for taking into account the extension of the fault plane.

*Ambato (1698/6/20)*

The Ambato earthquake (Fig. 15a) is one of the most destructive earthquakes of the colonial period. Damages were reported over an extended region, including the Tungurahua, Cotopaxi, and Chimborazo provinces. The earthquake occurred at night and several thousands of casualties were reported. The cities of Ambato and Latacunga were totally razed to the ground, whereas Riobamba (Antiguo) was partially demolished. Ambato was re-located after the earthquake. The event triggered a giant debris flow on the slopes of Carihuairazo Mountain that buried Ambato downstream. Some damage was also reported in Pichincha and Bolivar provinces. Only 17 intensities higher than IV are available, with maximum intensities reaching IX (Table 4). The intensity centre is located on the western slope of the Interandean Valley, however both slopes are possible locations of the epicentre according to the confidence contours. The magnitude interval is 7.2-7.9 if considering all locations within the 67% confidence contour. The large landslides at Carihuairazo favour a location of the epicentre on the western slope. A source close to Carihuairazo Mountain (on the 67% contour) would imply a $M_I$ 7.2 earthquake. No active fault has been previously identified in this area. The source of this earthquake might be the same fault system responsible for the much smaller Cusubamba (1962) and Pasa (1960) events, and may be part of the north-south thrust fault system. On the other hand, as the 67% confidence contour extends to the east and crosses the Interandean valley, a location on the Pallatanga fault system (or its extension to the north-east) located on the eastern side of the Carihuairazo cannot be excluded (yielding a magnitude $M_I$ 7.2-7.3). More multidisciplinary work (tectonic, paleoseismology, etc.) is required to identify the potential source of this destructive earthquake.

*Guayllabamba (1587/8/31)*

This earthquake struck northern areas of Pichincha province and southern towns of Imbabura province (Fig. 15b). The city of Quito was largely affected (churches and houses). Casualties and destruction were also reported in several villages north of Quito (Guayllabamba, Pomasqui), and extended all the way to Otavalo (intensity VII) in Imbabura. Although this earthquake is described by a few intensities (10 observations mainly within intensity degrees VII and VIII),

the confidence contours are quite narrow (10km×10km for contour 67%). The intensity centre is located north of Quito, suggesting rupture on a segment of the Quito fault system as the causative seismic source: either the Catequilla fault, the San Juan de Calderon fault or its extension to the north, or an unknown branch of the Quito fault system to the east. The magnitude is 6.4 at the intensity centre, and 6.35-6.55 at the 67% confidence level. Another possibility would be the Nono-Pululahua fault orientated NE-SW (same direction as the Otavalo fault) located west of the Quito fault system (intensity magnitude around 6.6) and crossing the 95% confidence contour.

## Studied events within the general geodynamic framework

For many years it has been recognized that the northwestern corner of South America is moving north-northeast as a block relative to the rest of the South American plate (Pennington, 1981; Kellogg et al, 1985) along a system of faults following the piedmont of the Eastern Andean Cordillera in Colombia, but obliquely crossing the Andean Ranges in Ecuador. The geodynamics of the northern Andes have been interpreted either as resulting from the obliquity of convergence between the Nazca and South American plates, or from the collision of the Carnegie Ridge with Ecuadorian margin (Ego et al, 1995), in any case with consequences that could be recognized along approximately 1400 km of escape tectonics (Trenkamp et al, 2002). The SW-NE trending right-lateral Pallatanga fault system (Fig. 16) probably constitutes the southern limit of the North Andean Block (NAB) which, starting from the Gulf of Guayaquil, crosses the Western Cordillera where the Interandean Valley can be first recognized (in the general area of the Riobamba basin). The Interandean Valley itself between Ambato and Quito appears to be a compressive N-S restraining bend (Lavenu et al, 1995; Ego et al, 1996), and constitutes a large left offset of the SW-NE strike-slip deformation. The right-lateral Chingual-Eastern Frontal and Romeral fault systems (Fig. 16, Romeral fault is in Colombia) constitute the deformation corridors further northeast of the Interandean Valley, the former being recognized as the eastern limit of the NAB further north (Tibaldi et al. 2007). For the Interandean Valley the concomitant E-W shortening proposed by Lavenu et al (1995) is kinematically consistent with the right lateral movement of the aforementioned strike-slip systems in an oblique convergence regime. It has been suggested that in the central Ecuadorian Andes the eastern limit of the NAB could be identified as a deformation corridor that, including the SW-NE Pallatanga fault trend, obliquely cuts the Eastern Cordillera along the Pisayambo earthquake

cluster (1ºS, 78ºW) and then turns northwards to meet the Chingual fault system 150 km to the north (Soulas et al, 1991). The N-S deformation corridor mostly shows a compressional regime with a small right lateral strike-slip component and is known as the Baeza-Reventador transpressive system (Gajardo et al, 2001).

Bearing in mind the depicted geodynamic framework for the Sierra, groups of earthquakes can be ascribed to different fault systems (Fig. 16). The Pepinales 1961, Cajabamba 1911, Riobamba 1797, Pelileo 1949, and the Tena 1987 (not examined in this study) earthquakes are distributed along the SW-NE Pallatanga-Pucara-Llanganates corridor. The Ambato 1698 earthquake could also have been generated along this corridor. All these events have intensity magnitudes larger than 6., with the largest being the large 1797 earthquake relocated at the southern edge of the Interandean Valley within this study. Two events (Due-Reventador 1955 and Salado-Reventador 1987) are localized further north in the Baeza Reventador transpressive system and show magnitudes greater than 6.5. There is no event assigned to the faster right-lateral strike-slip Chingual fault system in Ecuador, which is the northeastern continuation of the transpressive faults. The great 1834 Sibundoy earthquake, not analysed in this study, is probably located on this fault system 100 km north of the border between Ecuador and Colombia.

Starting from the south, the Pasa 1960, Cusubamba 1962, Pujili 1996, Pastocalle 1976, Toacazo 1944 and Aloasi 1976 earthquakes are located on the internal slopes of the Western Cordillera, very close to high Andes indigenous villages. The Guayllabamba 1587, Murco 1929 and Pomasqui 1990 events might also be included in this group. Their spatial distribution shows a clear N-S trend; focal mechanisms for the Pastocalle 1976 and Pujili 1996 events show N-S planes dipping to the west as probable focal solutions. These directions coincide with the N-S trend of the western limit of the restraining bend and confirm the compressional tectonics prevalent in the Interandean Valley. It is noteworthy that all of these events (except Guayllabamba) show magnitudes around five to six, and a recurrence time of less than 15 years during the XX$^{th}$ Century. The great 1698 Ambato earthquake could also be part of this group if located on the foot of the Western Cordillera, to the south of the Pasa epicentre. However, as indicated above, the small number of intensity points, their lack of good azimuthal coverage plus the event's very large intensity magnitude opens the possibility that the 1698 event may be related to the Pallatanga-Pucara-Llanganates group.

Both 1868 events (El Angel and Ibarra) and the 1955 Atahualpa event could be related to the southern prolongation of the Romeral Fault system or to a different set of faults running along the same SW-NE trend but located further west of the Romeral faults as suggested by Soulas et al (1991). The 1587 Guayllabamba event could also be ascribed to this group. These earthquakes related to the strike-slip faults also show magnitudes greater than 6. Finally a few historical events could be related to the eastern border of the restraining bend. This could be the case of the 1914 Antisana event ($M_{IC}$ 6.44); while the smaller 1938 Sangolquí and 1958 Latacunga (and 1929 Murco) events might be related to small structures that are localized in or enter obliquely in the Interandean Valley. The small 1990 Pomasqui earthquake could also fit in this category. These events have magnitudes in the range of five to six. At last, the 1859 earthquake might be a deep earthquake so no group is suggested for it.

## Conclusions

This is the first time an objective and reproducible method is applied for estimating the locations and magnitudes of historical earthquakes in the Sierra of Ecuador (covering the last 500 years). The Bakun & Wentworth (1997) grid-search method is applied. Spatial confidence contours corresponding to different probability levels delineate the possible locations of the intensity centre (equivalent to moment centroid), and the uncertainty on magnitude can be obtained from the distribution of the magnitudes of potential epicentres lying within given confidence contours. These uncertainty estimates will be taken into account in future seismic hazard studies. Nineteen crustal events of the Sierra are relocated, yielding equivalent moment magnitudes between 5.0 and 7.6 (Table 5). Bakun & Wentworth (1997) show that the method can be applied down to 5 observations. However, due to some difficulties inherent to the Ecuadorian data (mainly the spatial distribution), our study indicates that below 10 intensity assignments the results cannot be considered reliable. Furthermore, as shown in other applications of B&W (1997) technique (e.g. Bakun & Scotti 2006), the results show that the extension of the areas delineating the intensity centre location at different confidence levels is strongly dependent on the amount of intensity data, on their internal coherence, on the number of intensity degrees available, and on their spatial distribution in space.

To take into account the specificities of the Ecuadorian intensity dataset, and to understand their influence on the magnitude and location estimates, different sensitivity tests were performed:

- The distribution of intensities in space can be rather uneven, due to the sparsely inhabited mountain ranges. Intensities are mainly distributed in a north-south direction, following the axes of the Interandean valley, the main roads and the localisation of main cities and villages. One way of estimating the influence of this spatial distribution on the results is to use different spatial weighting. For all earthquakes, calculations were performed (1) without any weight and (2) with the weighting function initially proposed by B&W (1997) and used in nearly all applications of the method since then. This function gives higher weights to the points close to the assumed epicentre. In nearly all cases, the results are independent of the weighting chosen. The few exceptions concern very large magnitude events.
- Four large earthquakes display intensities higher or equal to IX (Pelileo 1949, Ibarra 1868, Riobamba 1797, Ambato 1698). Dealing with earthquakes of the XVI$^{th}$, XVII$^{th}$ and XVIII$^{th}$ centuries, these intensities can be over-estimated, due to a possible saturation at intensity degree VIII-IX and to the difficulty of assigning intensities to effects on nature. For these earthquakes, calculations were performed using intensities up to VIII, then up to IX, and so on. The results on locations and magnitudes are quite stable. However, magnitudes usually increase when including intensity degrees higher than X, therefore magnitudes of reference (Table 5) are always estimated with intensities up to IX.
- For very large earthquakes (equivalent moment magnitudes higher than 7.0), the hypothesis of a point source is no longer fulfilled, with possible over-estimation of the magnitude from the points located close to the fault plane. Therefore, calculations were performed after removing highest intensity degrees, that is observations located close to the assumed epicentre. Influence on the results appears rather limited for the location determination, but proved to be quite high for the magnitude estimation.

Interestingly, in the Ecuadorian Sierra characterized by “escape” compressional tectonics, where two major right-lateral strike-slip systems to the NE and SW are connected by a N-S trending restraining bend, large earthquakes seem to be related to the strike-slip faults, while the reverse faults of the western border of the restraining bend seem to produce only moderate

earthquakes no larger than M6. Large events M>6.5 have been generated along the transpressive system of the piedmont of the Eastern Cordillera.

Finally, this work aims at building a historical seismic catalogue homogeneous in magnitude, essential for any probabilistic seismic hazard assessment in Ecuador. We are currently working on a similar study for the coastal earthquakes. In the next years the on-going work on active tectonic faulting should provide new information on the potential active faults. Another important study will be to re-analyse the few earthquakes recorded by the international networks (in particular, the 1949, 1960, 1961 events); then more earthquakes would be available for the calibration. All these future findings might confirm or contradict the present results relying mostly on macroseismic intensities, and it is likely that further macroseismic analyses will have to be carried out in the light of this new information, deriving updated intensity attenuation models. Other methods than the Bakun and Wentworth (1997) will be worth applying, e.g. the method by Gasperini et al. (1999), and the different magnitude and location estimates obtained should be combined to determine the epistemic uncertainty (see Bakun 2010).

**Acknowledgments**

In charge of historical seismicity first at the Observatorio Astronómico and later at the Geophysical Institute in Quito since the early seventies, Jose Egred has contributed to this specific study and is naturally a co-author. Nonetheless, a special tribute must be paid for his long-lasting involvement in gathering and analysing historical documents, and building the intensity catalogue, which constitutes one of the fundamental foundations for all future seismic hazard studies led in Ecuador. Besides, we are grateful to R. Stein and W. Mooney who made interesting and stimulating comments on an earlier version of the manuscript. We thank the editor Andrew Curtis and two anonymous reviewers for insightful evaluations of the manuscript and constructive suggestions. Programs and figures rely on Mathematica (http://www.wolfram.com/). J. Aguilar, E. Pathier and C. Lasserre kindly helped us for producing some of the figures. This work has been partially supported by the ADN project (Andes du Nord) from the Agence Nationale de la Recherche under the Contract Number ANR-07-BLAN-143.

**Affiliations**

LGIT
IRD-UJF-CNRS
BP 53
38041 Grenoble Cedex 9
France
C.B.

Instituto Geofísico
Escuela Politécnica Nacional
Ladrón de Guevara E11-253
Apartado 2759 – Quito
Ecuador
H.Y., J.E., A.A., J-C.S.

USGS
Menlo Park
CA — US
W.H.B.

**References:**

Alvarado, A., 2009. Mapa de fallas y pliegues quanternarios del Ecuador, database, Instituto Geofisico, Escuela Politecnica Nacional, Internal Report.

Ambraseys, N.N., 2001. Reassessment of earthquakes, 1900-1999, in the Eastern Mediterranean and the Middle East, *Geophys. J. Int*, 145, 471-485.

Ambraseys, N.N. & Bilham, R., 2003. Reevaluated intensities for the great Assam earthquake of 12 June 1897, Shillong, India, *Bull. Seism. Soc. Am*. 93, 665-673.

Ambraseys, N. & Douglas, J., 2004. Magnitude calibration of Northern Indian earthquakes, *Geophys. J. Int.* **159,** 165–206.

Atkinson, G.M. & Wald, D.J., 2007. "Did you feel it?" Intensity data: a surprisingly good measure of earthquake ground motion, *Seismological Research Letters*, 78, 3, 362-368.

Azzaro, R., Barbano, M.S., D'Amico S. & Tuve, T., 2006. The attenuation of seismic intensity in the Etna region and comparison with other Italian volcanic districts, *Annals of Geophysics*, Vol. 49, N°4/5, 1003-1005.

Bakun, W.H., 2010. Estimating epistemic uncertainty for historical earthquakes, Seismological Society of America, Annual Meeting, Portland, Oregon, 21-23 April, abstract submitted.

Bakun, W.H. & Wentworth, C.M., 1997. Estimating earthquake location and magnitude from Seismic Intensity Data, *Bull. Seism. Soc. Am*., 87, 6, 1502-1521.

Bakun, W.H. & Wentworth, C.M., 1999. Erratum to Estimating earthquake location and magnitude from seismic intensity data, *Bull. Seism. Soc. Am*. 89, 557.

Bakun, W.H., 1999. Seismic activity of the San Francisco Bay Region, *Bull. Seism. Soc. Am*., 89, 3, 764-784.

Bakun, W.H. & Hopper, M.G., 2004. Magnitudes and locations of the 1811–1812 New Madrid, Missouri, and the 1886 Charleston, South Carolina, earthquakes, Bull. Seism. Soc. Am. 94, 64–75.

Bakun, W.H., 2005. Magnitude and location of historical earthquakes in Japan and *implications* for the 1855 Ansei Edo Earthquake. *J*. *Geophys*. *Res*., 110, B02304, doi:10.1029/2004JB003329.

Bakun, W.H., & O., Scotti, 2006. Regional intensity attenuation models for France and the estimation of magnitude and location of historical earthquakes, *Geophys. J. Int.*, 164, 596-610.

Beauval, C., & O., Scotti, 2004. Quantifying sensitivities of Probabilistic Seismic Hazard Assessment for France to earthquake catalogue uncertainties, truncation of ground-motion variability and magnitude limits, Bull. Seism. Soc. Am., 94(5), 1579-1594.

Beauval, C., & Scotti, O., 2003. Mapping b-values in France using two different magnitude ranges: possible non power-law behavior, Geophys. Res. Lett., 30(17), 1892, doi:10.1029/2003GL017576.

Centro Regional de Sismologia para America del Sur (CERESIS), 1985. Proyecto SISRA (Programa para la mitigación de efectos de los Terremotos en la Región Andina) - Ecuador, datos de hipocentros e intensidades, Vol 6, 175p.

CND/NRC (Committee on Natural disaster/National Research Council), 1991. The March 5, 1987, Ecuador Earthquakes: Mass Wasting and Socioeconomic Effects, Commission on Engineering and Technical Systems, 184 pages.

Efron, B., 1982. The jackknife, the bootstrap and other resampling plans, in CBMS-NSF Regional Conference Series in Applied Mathematicas, Society for Industrial and Applied Mathematics, Philadelphia, 92 pp.

Ego, F., Sébrier, M. & Yepes, H., 1995. Is the Cauca-Patia and Romeral Fault System left or rightlateral?, *Geophys. Res. Lett.*, 22(1), 33–36.

Ego, F., Sébrier, M., Lavenu, A., Yepes H. & Egüez, A., 1996. Quaternary state of stress in the Northern Andes and the restraining bend model for the Ecuadorian Andes, *Tectonophysics*, 259, 101-116.

Egred, J., 2009a. Terremotos del Ecuador, dos volumen, Escuela Politecnica Nacional, Instituto Geofisico, internal report.

Egred, J., 2009b. Catalogo de terremotos del Ecuador 1541-2009, Escuela Politecnica Nacional, Instituto Geofisico, internal report.

Egred, J., 2000. El terremoto de Riobamba, Ediciones Abya-Yala, Tomo 2, 107 pp.

Egred, J., 2004. Terremoto de Riobamba del 4 de Febrero de 1797, Investigaciones en Geociencias, A. Alvarado, A. Garcia-Aristizabal, P. Mothes, M. Segovia Editores, Vol. 1, 67-86.

Egüez, A., Alvarado, A., Yepes, H., Machette, M.N., Costa, C., & Dart, R.L., 2003. Database and map of quaternary faults and folds of Ecuador and its offshore regions, *USGS Open-File Report* 03-289.

Engdahl, E.R. & Villaseñor, A., 2002. Global Seismicity: 1900–1999, in W.H.K. Lee, H. Kanamori, P.C. Jennings, and C. Kisslinger (editors), International Handbook of Earthquake and Engineering Seismology, Part A, Chapter 41, pp. 665–690, Academic Press.

Engdahl, E.R., van der Hilst, R. & Buland, R., 1998. Global teleseismic earthquake relocation with improved travel times and procedures for depth determination, *Bull. Seism. Soc. Am.* 88, 722–743.

Escuela Politecnica Nacional, 1990. Informe de actividades 1989-1990, Instituto Geofisico, Quito, 92 pp.

Espinosa, A.F., Hall, M.L. & Yepes, H., 1991a. Tectonics and seismicity. In: R.L. Schuster (Editor), The March 5, 1987, Ecuador Earthquakes—Mass Wasting and Socioeconomic Effects. Natural Disaster Studies, National Academy of Sciences, National Academy Press, Washington, D.C., 5, 29-41.

Espinosa, A.F., Egred, J. García-López, M. and Crespo, E., 1991b. Intensity and damage distribution. In: R.L. Schuster (Editor), The March 5, 1987, Ecuador Earthquakes—Mass

Wasting and Socioeconomic Effects. Natural Disaster Studies, National Academy of Sciences, National Academy Press, Washington, D.C., 5, 42-50.

Esteva, L. (1968). Regionalización sísmica de México para fines de Ingeniería, *Ph. D. Thesis*, School of Engineering, National Autonomous University of Mexico (UNAM).

Gajardo, E., Yepes, H., Ramon,P., Hall, P., Mothes P. & J., Aguilar, 2001. Evaluacion del peligro sismico para la ruta del OCP y evaluacion complementaria del peligro volcanico, Escuela Politecnica Nacional, Instituto Geofisico, internal report.

Gasperini, P., Bernardini, F., Valensise G. & Boschi, E., 1999. Defining seismogenic sources from historical earthquake felt reports, *Bull. Seism. Soc. Am*, 89, 94-110.

Gutenberg, B. & Richter, C.F., 1956. Earthquake magnitude, intensity, energy and acceleration, *Bull. Seism. Soc. Am*, 46, p. 105-145.

Hall, M.L. & Wood, C.A., 1985. Volcano-tectonic segmentation of the northern Andes, *Geology*, v. 13, 203-207.

Harvard Seismology, 2009. Centroid Moment tensor (CMT) catalog search, http://www.seismology.harvard.edu/(last accessed August 2009).

Hinzen, K.-G. & Oemisch, M., 2001. Location and magnitude from seismic intensity data of recent and historic earthquakes in the Northern Rhine area, central Europe, *Bull. Seism. Soc. Am*., 91, 40–56.

Kawakatsu, H. & Proaño Cadena, G., 1991. Focal mechanisms of the March 6, 1987 Ecuador Earthquakes – CMT Inversion with a First Motion Constraint, *J. Phys. Earth*., 39, 589-597.

Kellogg, J.N., Ogujiofor, I.J. & Kansaka, D.R., 1985. Cenozoic tectonics of the Panama and North Andes blocks. Memorias - Congreso Latinoamericano de Geologia 6, 34-49.

Lavenu, A., Winter, T. & Dávila, F., 1995. A Plio-Quaternary compressional basin in the Interandean Depression, Central Ecuador. *Geophys. J. Int*., 121, 279-300.

Ramirez, E., 1951. El gran terremoto ecuatoriano de Pelileo, Revista Academia Colombiana, Ciencias exactas, Fisicas y naturales, v. 8, p. 126-136.

Meltzner, A.J. & Wald, D.J., 1999. Foreshocks and aftershocks of the Great 1857 California earthquake, *Bull. Seism. Soc. Am.*, 89, 1109-1120.

Musson, R. M. W., and Jiménez, M-J. 2008. Macroseismic estimation of earthquake parameters. NERIES project report, Module NA4, Deliverable D3.

McGuire, R.K. (2008). Probabilistic seismic hazard analysis: Early history (a Review), *Earthquake Engng. Struct. Dyn.,* 37, 329-338.

Nieto, A.S., 1991. Mass wasting and flooding. In: R.L. Schuster (Editor), The March 5, 1987, Ecuador Earthquakes—Mass Wasting and Socioeconomic Effects. Natural Disaster Studies, National Academy of Sciences, National Academy Press, Washington, D.C., 5, 23-28.

Palme de Osechas, C., Morandi, M.T. & Choy, J.E., 2005. Re-evaluacion de las intensidades de los grandes sismos historicos de la region de la cordillera de Mérida utilizando el método de Bakun and Wentworth, *Revista Geografica Venezolana*, 233-253.

Parsons, T., 2004. Recalculated probability of M≥7 earthquakes beneath the Sea of Marmara, Turkey, *J. Geophys. Res*., 109, B05304, doi:10.1029/2003JB002667.

Pasolini, C., Gasperini, P., Albarello, D., Lolli, B. & D'Amico, V., 2008. The attenuation of seismic intensity in Italy, Part I: Theoretical and empirical backgrounds, *Bull. Seism. Soc. Am.*, 98, 682-691.

Pennington, W. D., 1981. Subduction of the Eastern Panama Basin and Seismotectonics of Northwestern South America, *J. Geophys. Res*., 86(B11), 10,753–10,770.

Singaucho, J-C., 2009. Mapa de máximas intensidades sísmicas del Ecuador. Criterios estructurales para mejorar la estimación de intensidades. Proyecto de Titulación, Facultad de Ingeniería Civil y Ambiental, Escuela Politécnica Nacional, 219 pp.

Soulas, J-P., Ramón, P., Eguez, A., Alvarado, A., Yepes, H. and Gajardo, E., 2001. Evaluacion de las fallas activas que cruzan el trazado del OCP, Instituto Geofisico, Escuela Politecnica Nacional, Internal Report (TECHINT LTD.).

Soulas, J-P., Eguez, A., Yepes, H. & Perez, H., 1991. Tectonica activa y riesgo sismico en los Andes Ecuatorianos y el extremo Sur de Colombia*, Bol. Geol. Ecuat.,* Vol. 2, N°1, 3-11.

Tibaldi, A., Rovida, A., Corozzato, C., (2007). Late Quaternary kinematics, slip-rate and segmentation of a major Cordillera-Parallel transcurrent fault: the Cayambe-Afiladores-Sibundoy system, NW south America, *Journal of Structural Geology, 29(4),* 664-680.

Trenkamp, R., Kellogg, J.N., Freymueller, J.T. & Mora, H.P, 2002. Wide plate margin deformation, southern Central America and northwestern South America, CASA GPS observations, *Journal of South American Earth Sciences*, 157-171.

United States Geological Survey / National Earthquake Information Center, 2009. Preliminary Determination of Epicentres (PDE) catalog search, http://earthquake.usgs.gov/regional/neic/, last accessed August 2009).

Wells, D. L., & Coppersmith, K. J., 1994. New empirical relationships among magnitude, rupture length, rupture width, rupture area, and surface displacement, *Bull. Seism. Soc. Am.* 84 , 974 – 1002.

Winter, T., 1990. Mécanismes des déformations récentes dans les Andes équatoriennes. These Univ. Paris-Sud, Orsay, 205 pp.

Woodward-Clyde Consultants, 1981. Investigations for the studies of seismic risk for the Agoyan dam site, Report for the Agoyan Hydroelectric project of the Instituto Ecuatoriano de Electrificación (INECEL), 85 pp.

## Tables

### Table 1. Calibration and test earthquakes

| Event No. | Event Name | Yr/Mo/Day | Instr. Latitud | Instr. Longitud | Source | M | Source |
|---|---|---|---|---|---|---|---|
| 1* | Pujili | 1996/3/28 | -1.044 | -78.724 | EPN catalog | 5.9 $M_w$ | HRV |
| 2* | Pomasqui | 1990/8/11 | -0.0392 | -78.4274 | EPN (EPN, 1990) | 5.3 $M_w$ | CMT |
| 3* | Salado-Reventador | 1987/3/6 | -0.087 | -77.814 | EPN (Gajardo et al. 2001) | 7.1 $M_w$ | HRV |
| 4* | Pastocalle | 1976/10/6 | -0.727 | -78.734 | EHB | 5.7 $M_b$ | ISC |
| 5 | Due-Reventador | 1955/5/11 | -0.200 | -77.800 | EHB | 6.8 | UK |
| 6 | Pepinales | 1961/4/8 | -2.0890 | -78.9680 | EHB | - | - |
| 7 | Pelileo | 1949/8/5 | -1.23 | -78.405 | Woodward-Clyde, 1981 | 6.8 $M_s$ | UK GR (EHB) |

*Calibration event; otherwise test event.
EPN : determination by the Escuela Politecnica Nacional – Instituto Geofisico – Quito
EHB : relocated by Engdahl and Villasenor (2002) using the method Engdahl, van der Hilst and Buland (1998)

### Table 2. Intensity data for calibration and test events: median hypocentral distances* used in calibration

| Event No. | III | IV | V | VI | VII | VIII | XIX | X | No. of MSKI ≥ III |
|---|---|---|---|---|---|---|---|---|---|
| 1 | 76.9 | 55.1 | 31.8 | 23.5 | 13.1 | - | - | - | 87 |
| 2 | - | 25.3 | 17.9 | 13.4 | - | - | - | - | 66 |
| 3 | - | - | - | 73.8 | 54.5 | 34.3 | 24.1 | - | 228 |
| 4 | - | 59.8 | 28.1 | 21.2 | 15.3 | - | - | - | 72 |
| 5 | Test event (magnitude determination only) | | | | | | | | 22 |
| 6 | Test event (location determination only) | | | | | | | | 31 |
| 7 | Test event | | | | | | | | 82 |

* Median distances are used only when there is no doubt on the spatial completeness of the intensity degree (and with a minimum of 7 intensity assignments).

**Table 3. Calibration and test events – results from applying Bakun & Wentworth (1997) analysis.**

| Event No. | Event Name | Yr/Mo/Day | M | Source | $M_I$** | $M_I$*** | Δ# km | FL km | Width km |
|---|---|---|---|---|---|---|---|---|---|
| 1* | Pujili | 1996/3/28 | 5.9 $M_w$ | HRV | 5.85 | 5.97 | 8.4 | 11 | 7.5 |
| 2* | Pomasqui | 1990/8/11 | 5.3 $M_w$ | CMT | 5.28 | 5.4 | 7.1 | 4.9 | 4.8 |
| 3* | Salado-Reventador | 1987/3/6 | 7.1 $M_w$ | HRV | 6.96 | 7.0 | 4.2 | 56 | 18 |
| 4* | Pastocalle | 1976/10/6 | 5.7 $M_b$ | ISC | 5.8 | 5.89 | 5.9 | 8.4 | 6.5 |
| 5 | Due-Reventador | 1955/5/11 | 6.8 | UK | 7 | 6.9 | 5.9 | 37 | 14.7 |
| 6 | Pelileo | 1949/8/5 | 6.8 $M_s$ | UK GR | 6.6 | 6.3 | 21 | 37 | 14.7 |
| 7 | Pepinales | 1961/4/8 | - | - | 6.3 | 6.5 | 10 | 18.9 | 10.1 |

*Calibration event; otherwise test event.
** Evaluated at the epicentre
*** Evaluated at intensity centre
Δ# Distance from the epicentre to the intensity centre
FL is subsurface rupture length, FL and downdip rupture width are estimated from the instrumental magnitude (Wells & Coppersmith, 1994, generic equation)

**Table 4: Historical earthquakes: number of data per intensity degree (II is not used in calculations) based on the intensity historical catalogue (Egred, 2009b).**

| Yr/Mo/Day | Event Name | II | III | IV | V | VI | VII | VIII | IX | X | XI | **Total** |
|---|---|---|---|---|---|---|---|---|---|---|---|---|
| 1955/5/11 | Due-Reventador | 4 | 1 | 1 | 1 | 10 | 5 | - | - | - | - | **22** |
| 1949/8/5 | Pelileo | - | 7 | 15 | 10 | 14 | 12 | 11 | 7 | 6 | - | **82** |
| 1976/11/29 | Aloasi | 4 | 6 | 4 | 5 | 9 | 6 | - | - | - | - | **34** |
| 1962/11/16 | Cusubamba | - | 2 | 2 | 1 | 3 | 3 | - | - | - | - | **11** |
| 1961/4/8 | Pepinales | - | 1 | 5 | 5 | 9 | 8 | 3 | - | - | - | **31** |
| 1960/7/30 | Pasa | - | 3 | 10 | 4 | 4 | 6 | - | - | - | - | **27** |
| 1958/1/24 | Latacunga | 1 | 7 | 1 | 1 | 4 | - | - | - | - | - | **14** |
| 1955/7/20 | Atahualpa | | 4 | 3 | - | 10 | 23 | 5 | - | - | - | **45** |
| 1944/9/15 | Toacazo | 2 | 2 | 3 | 1 | 10 | 3 | - | - | - | - | **21** |
| 1938/8/10 | Sangolqui | - | 8 | 4 | 3 | 10 | 13 | 2 | - | - | - | **40** |
| 1929/7/25 | Murco | 2 | 3 | 2 | 4 | 1 | 9 | 1 | - | - | - | **24** |
| 1914/5/31 | Antisana | - | 11 | 10 | 6 | 3 | 9 | 6 | - | - | - | **45** |
| 1911/9/23 | Cajabamba | 1 | 2 | 1 | - | 4 | 9 | 1 | - | - | - | **18** |
| 1868/8/15 | El Angel | - | 1 | 1 | - | - | 3 | 8 | | | | **15** |
| 1868/8/16 | Ibarra | - | 1 | 5 | 2 | 4 | 9 | 24 | 26 | - | - | **71** |
| 1859/3/22 | Quito | - | 5 | 2 | 1 | 2 | 18 | 1 | - | - | - | **30** |
| 1797/2/4 | Riobamba | - | 9 | 2 | 1 | 1 | 11 | 34 | 19 | 37 | 3 | **117** |
| 1698/6/20 | Ambato | 2 | 1 | - | - | 3 | 1 | 7 | 6 | - | - | **20** |
| 1587/8/31 | Guayllabamba | - | - | - | - | 1 | 6 | 3 | - | - | - | **10** |

**Table 5. Historical earthquakes: results.**

| Yr/Mo/Day | Event Name | Lat.¥ of IC | Long.¥ of IC | $M_{IC}$ * | $M_{IC}$: 67%** | FL*** (km) |
|---|---|---|---|---|---|---|
| 1976/11/29 | Aloasi | -0.52 | -78.61 | 5. | 5.0-5.2 | 3.2 |
| 1962/11/16 | Cusubamba | -1.16# | -78.65# | 5.8-6.# | - | 13 |
| 1960/7/30 | Pasa | -1.20# | -78.7# | 5.6-5.7# | - | 7.3 |
| 1958/1/24 | Latacunga | -0.98 | -78.59 | 5.0 | 4.9-5.2 | 3.3 |
| 1955/7/20 | Atahualpa | 0.28 | -78.39 | 6.14 | 6.1-6.3 | 15.2 |
| 1944/9/15 | Toacazo | -0.71# | -78.7# | 5.6-5.8# | - | 8.4 |
| 1938/8/10 | Sangolqui | -0.4 | -78.41 | 5.8 | 5.6-6.0 | 9.6 |
| 1929/7/25 | Murco | -0.5 | -78.48 | 5.88 | 5.8-6.1 | 10.7 |
| 1914/5/31 | Antisana | -0.6 | -78.42 | 6.44 | 6.4-6.5 | 22.9 |
| 1911/9/23 | Cajabamba | -1.73# | -78.8# | 6.1-6.3# | - | 16.5 |
| 1868/8/15 | El Angel | 0.7 | -77.92 | 6.6 | 6.4-6.8 | 28.4 |
| 1868/8/16 | Ibarra | 0.38 | -78.43 | 7.25 | 7.1-7.7 | 70.7 |
| 1859/3/22 | Quito | 0.02 | -78.75 | 7.2 | 6.9-7.3 | 64 |
| 1797/2/4 | Riobamba | -1.5 | -78.6 | 7.6 | 7.5-7.9 | 110.7 |
| 1698/6/20 | Ambato | -1.4# | -78.8# | 7.2-7.3# | - | 64 |
| 1587/8/31 | Guayllabamba | 0.05 | -78.33 | 6.4 | 6.35-6.55 | 21.7 |

*Intensity magnitude obtained at the intensity centre.

# Intensity magnitude at a preferred location for the earthquake epicentre, which is not the intensity centre (see text).

** intensity magnitude confidence range: range of magnitudes of epicentres contained within the 67% confidence contour.

¥ note that the precision on the latitude and longitude is dependent on the spatial grid step (varying between 0.025° and 0.05°)

***FL: Subsurface rupture length according to magnitude at intensity centre (and generic equation from Wells & Coppersmith, 1994)

**Table 6. Names and acronyms of faults mentioned in the text and displayed on the maps.**

| Acronym of the fault | Fault (or fault system) name |
|---|---|
| AL | Alaquez Fault |
| AF | Apuela Fault |
| CF | Catequilla Fault |
| EAF | El Angel fault |
| GHFS | Guamote-Huigra Fault System |
| HFS | Huayrapungo Fault System |
| LVF | La Victoria Fault |
| MF | Machachi Fault |
| MiF | Mira Fault |
| MuF | Mundug Fault |
| NFS | Nanegalito Fault System |
| NPF | Nono-Pululahua Fault |
| OF | Otavalo Fault |
| PF | Pucara Fault |
| PFS | Pallatanga Fault System |
| PiF | Pintag Fault |
| QFS | Quito Fault System |
| RP | Reventador Fault |
| SF | Salado Fault |
| SJF | San Juan de Calderon Fault |
| SPYFS | Poalo- Saquisili-Yambo Fault System |
| TF | Toacazo Fault |
| TuF | Tufiño Fault |

# Figures

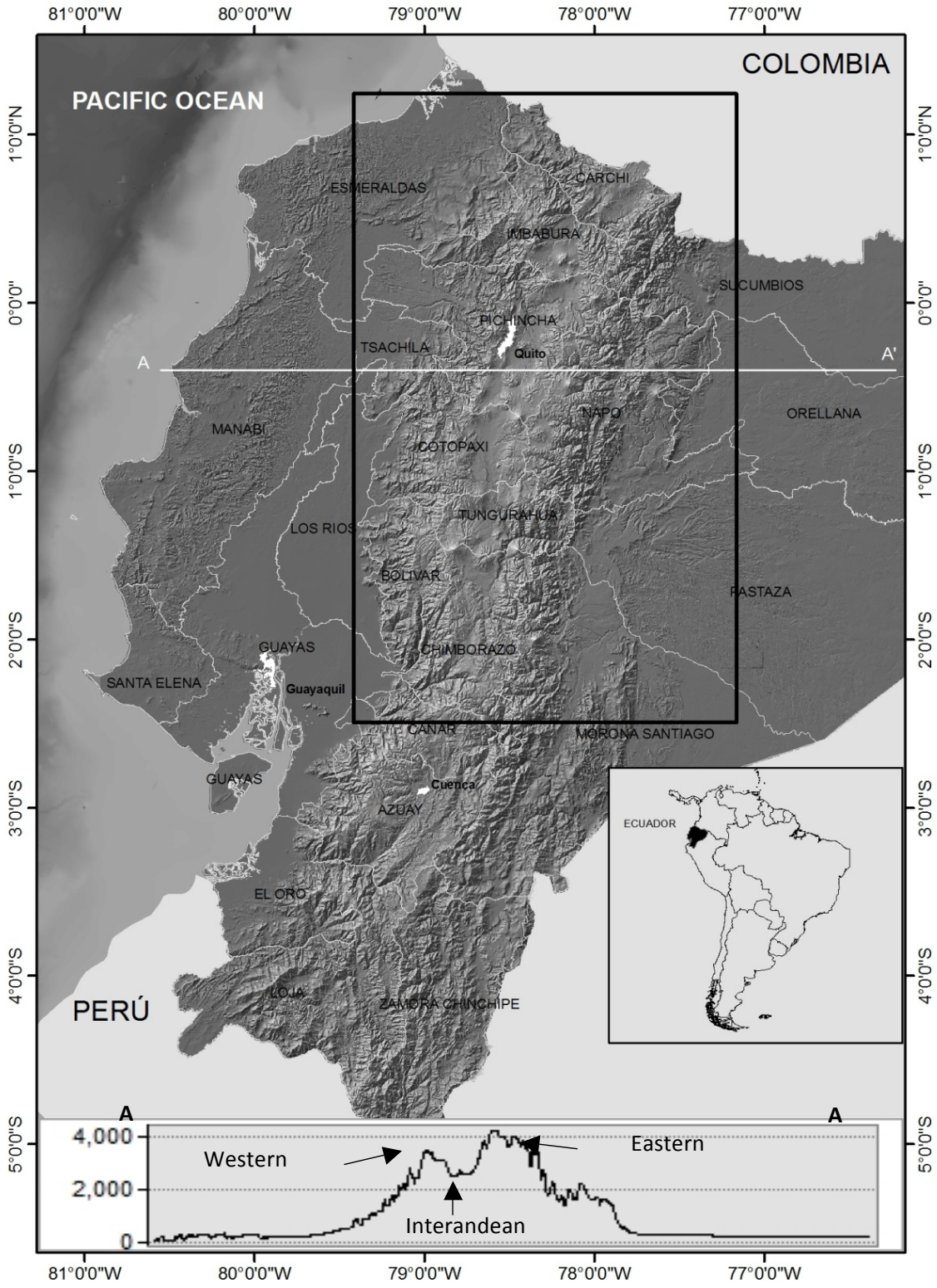


Figure 1: Ecuador and the region under study (rectangle). A-A' is a topographic profile showing the Interandean Valley and both bordering mountain ranges: the Western and Eastern Cordilleras. Province names mentioned throughout the paper are indicated.

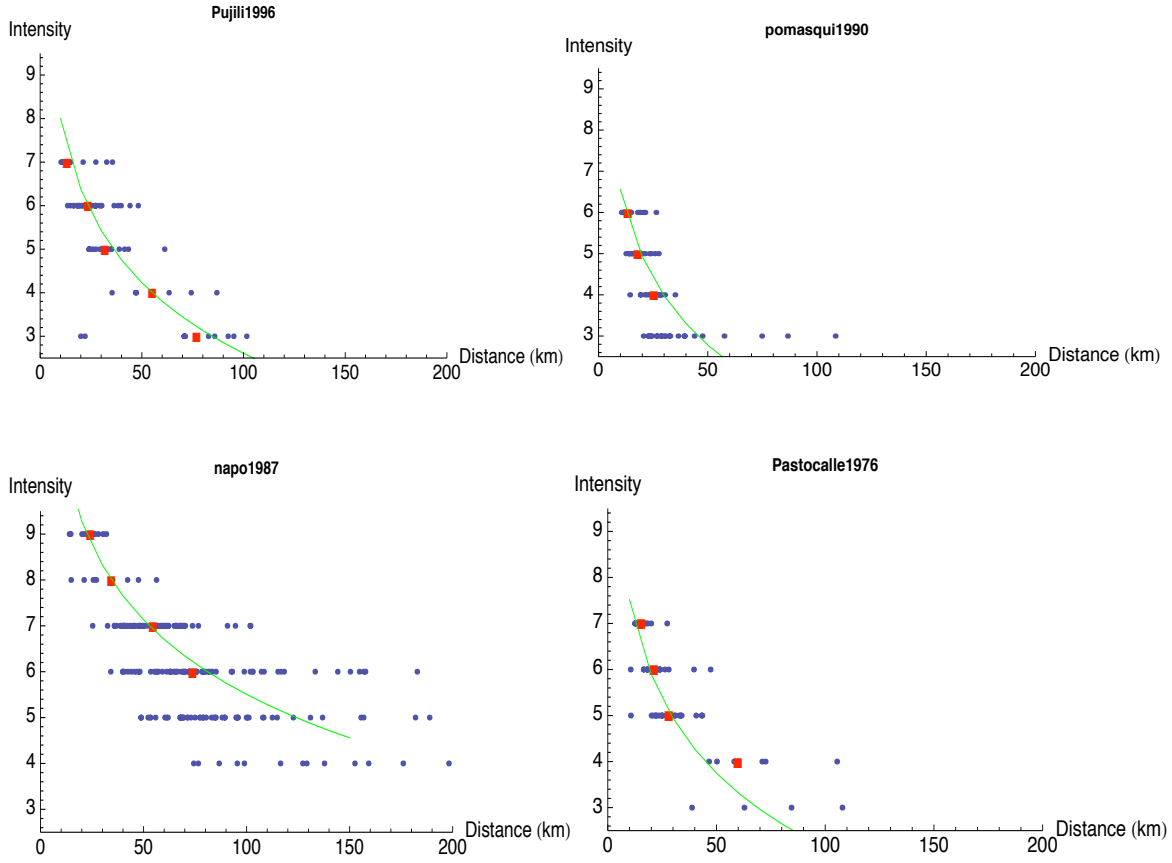


Figure 2: Intensity data for the calibrating events (Table 1). Blue dots: intensity observations. Red squares: median distances (see Table 2). Green curve: attenuation model (Eq. 2). Distance is hypocentral, with a generic depth fixed to 10 km.

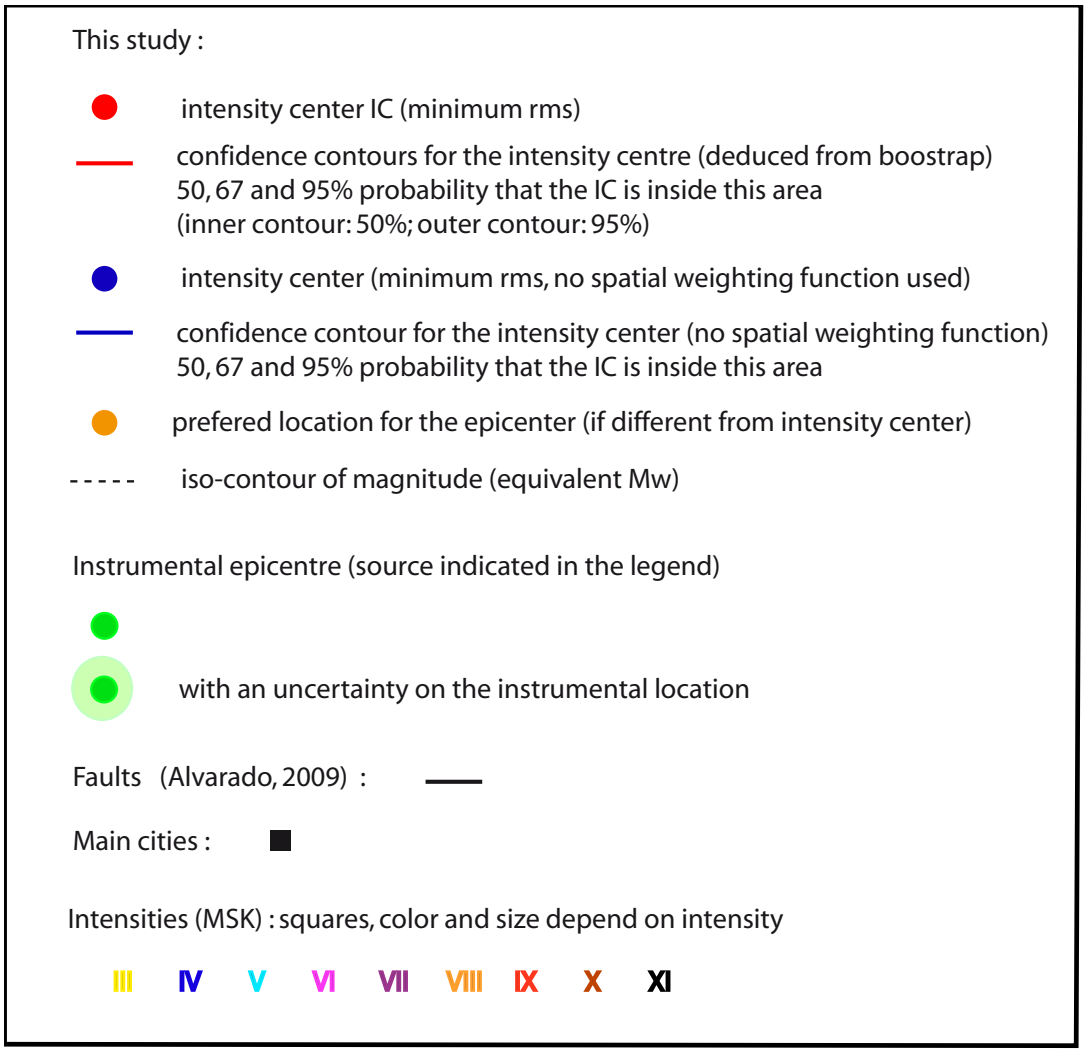


Figure 3: Detailed legend for Figure 4 and Figures 6 to 15.

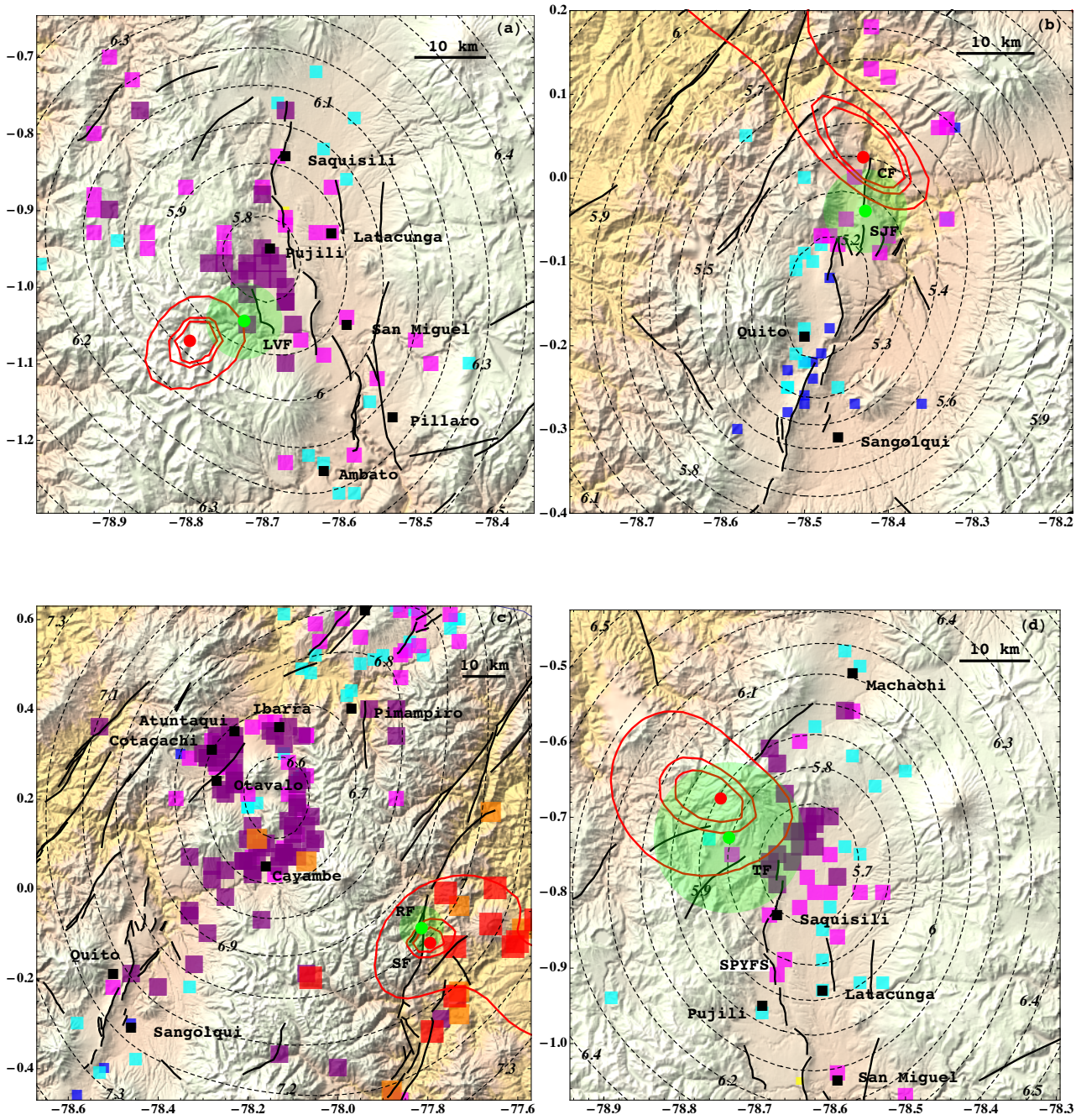


Figure 4: Determination of magnitude and location for calibrating events (Table 3): (a) Pujili ($M_W$ 5.9, 1996); (b) Pomasqui ($M_W$ 5.3, 1990); (c) Napo ($M_W$ 7.1, 1987); (d) Pastocalle ($M_b$ 5.7, 1976). LVF, CF, SJF, RF, SF, MF and TF are faults (Table 6). See Legend in Fig. 3. Topography: SRTM data from http://srtm.csi.cgiar.org/.

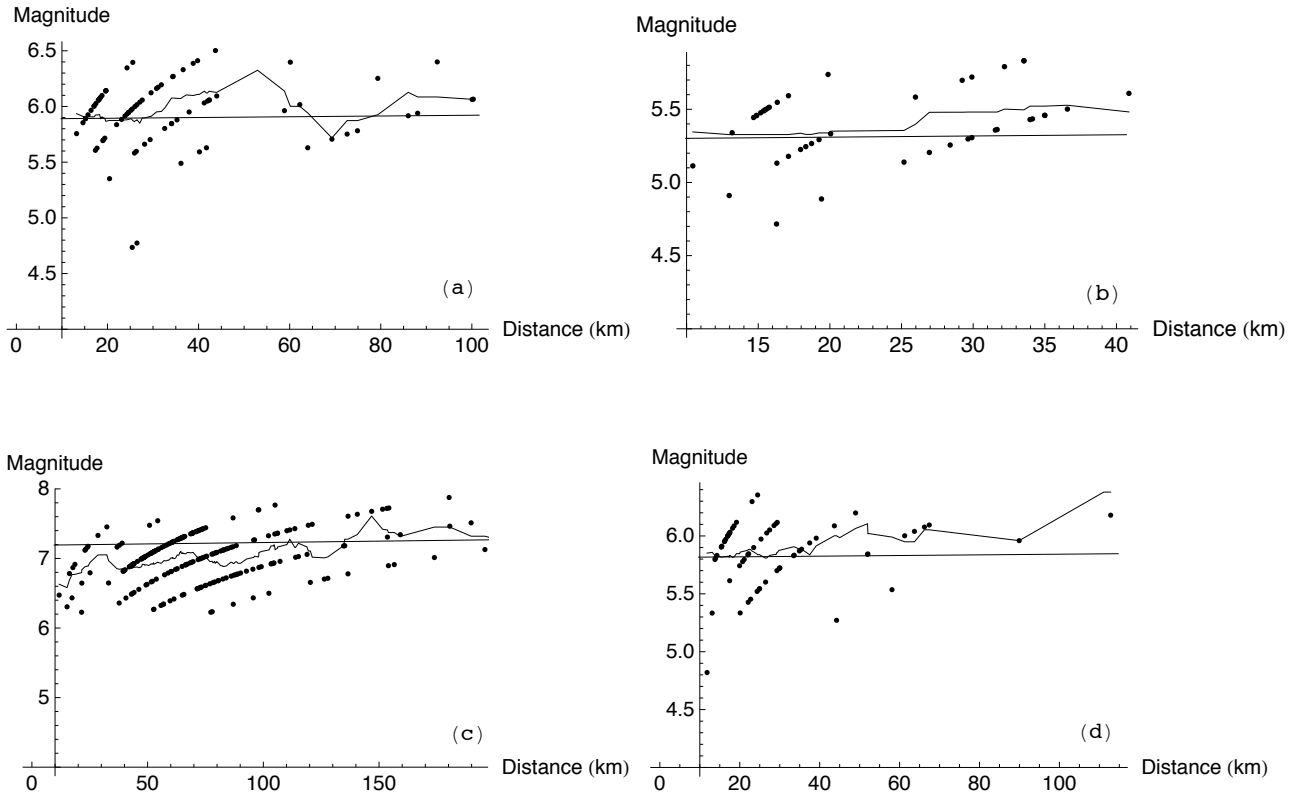


Figure 5: Calibrating events: magnitudes calculated from all intensity observations using Eq. 1, versus hypocentral distances calculated based on the intensity centre. (a) Pujili; (b) Pomasqui; (c) Salado-Reventador; (d) Pastocalle. Curve: moving average over 10km-width distance intervals. Horizontal line: instrumental magnitude $M_w$ (except for Pastocalle event, $M_b$).

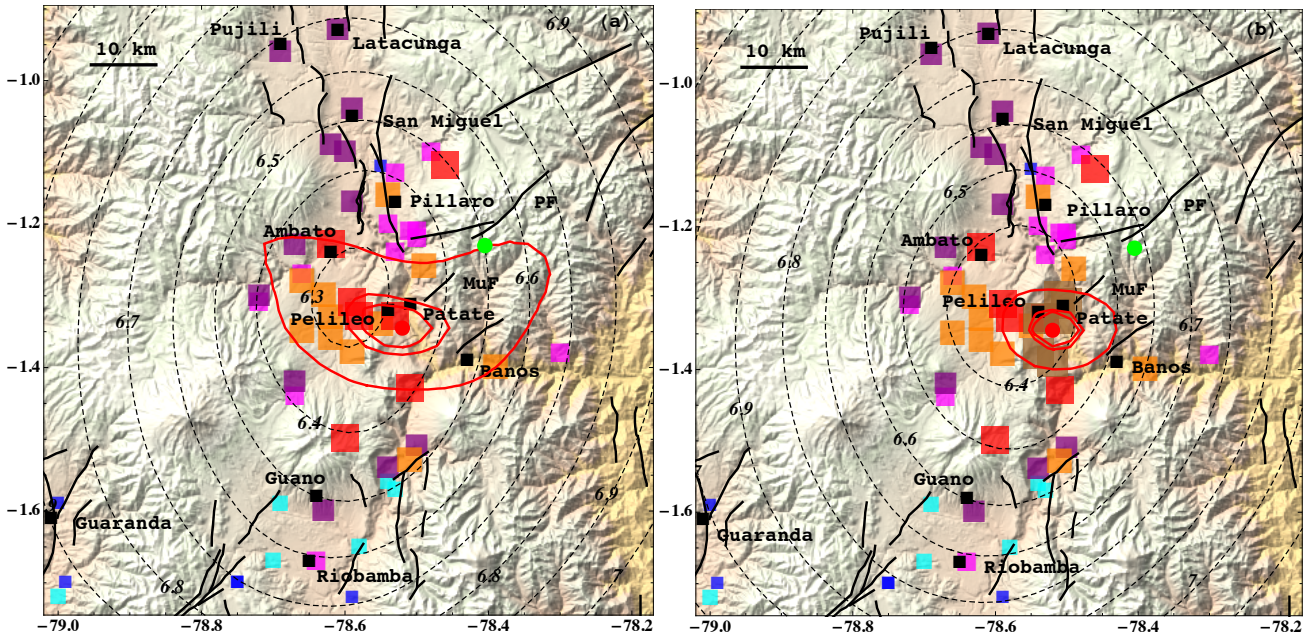


Figure 6: Determination of magnitude and location for Pelileo historical event (1949, $M_{G\text{-}R}$ 6.8): (a) using intensities up to IX; (b) including intensities X. Instrumental location from Woodward-Clyde (1981). The uncertainty on the instrumental location is not known. PF and MuF are Pucara and Mundug faults (Table 6). See Legend in Figure 3.

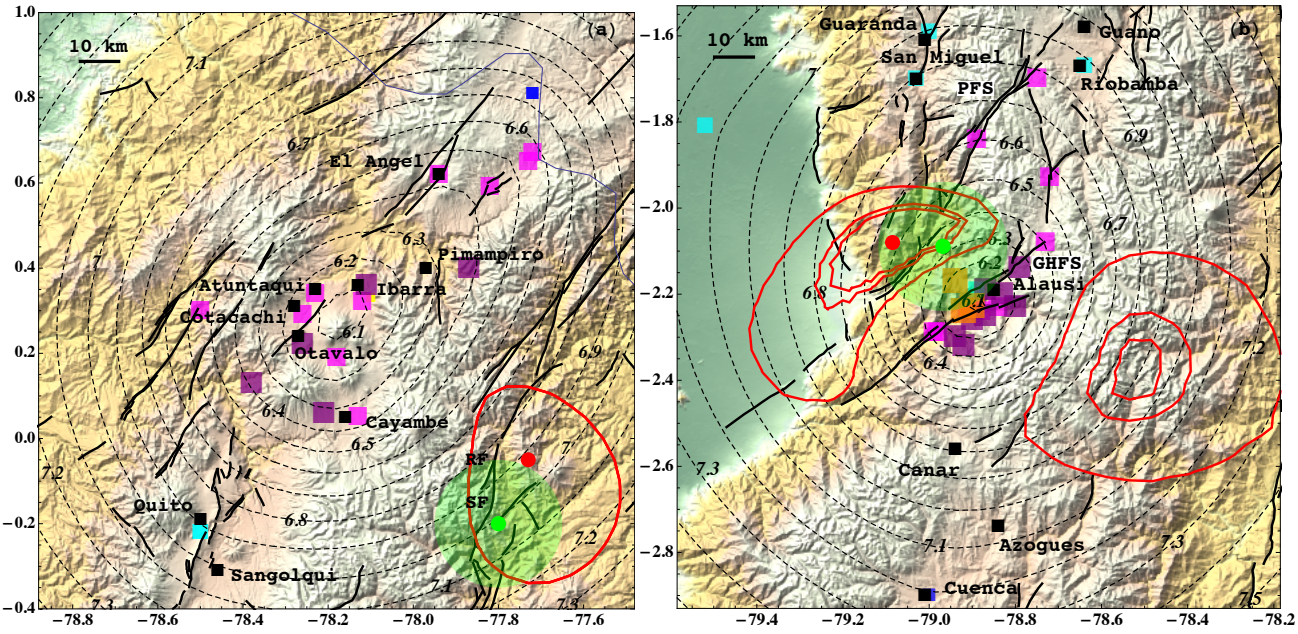


Figure 7: Determination of magnitude and location for (a) Due-Reventador (1955, $M_{UK\text{-}PAS}$ 6.8, EHB) and (b) Pepinales (1961, EHB, no instrumental magnitude). No reliable confidence contour can be obtained for Due-Reventador (red contour is 10%). RF, SF, PFS, GHFS are faults (Table 6). See Legend in Figure 3. Results reported in Table 5.

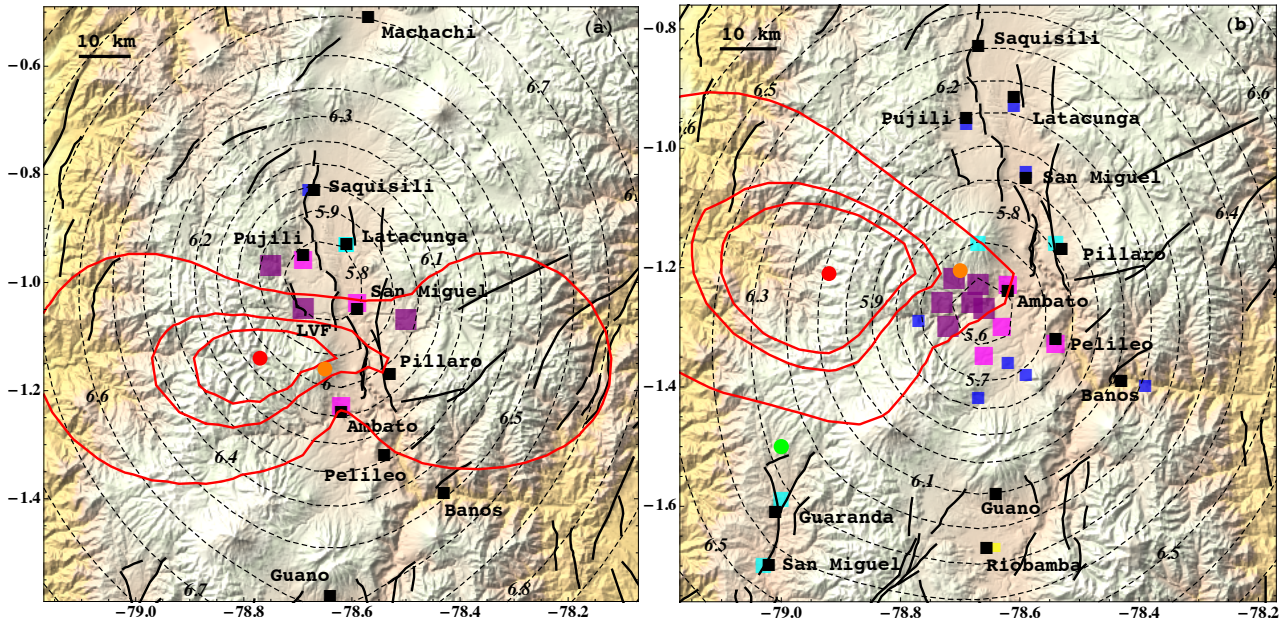


Figure 8: Determination of magnitude and location for historical events. (a) Cusubamba (1962). (b) Pasa (1960), instrumental epicentre from CGS (certainly bearing at least 30km uncertainty). LVF is La Victoria fault (Table 6). See Legend in Figure 3. Results reported in Table 5.

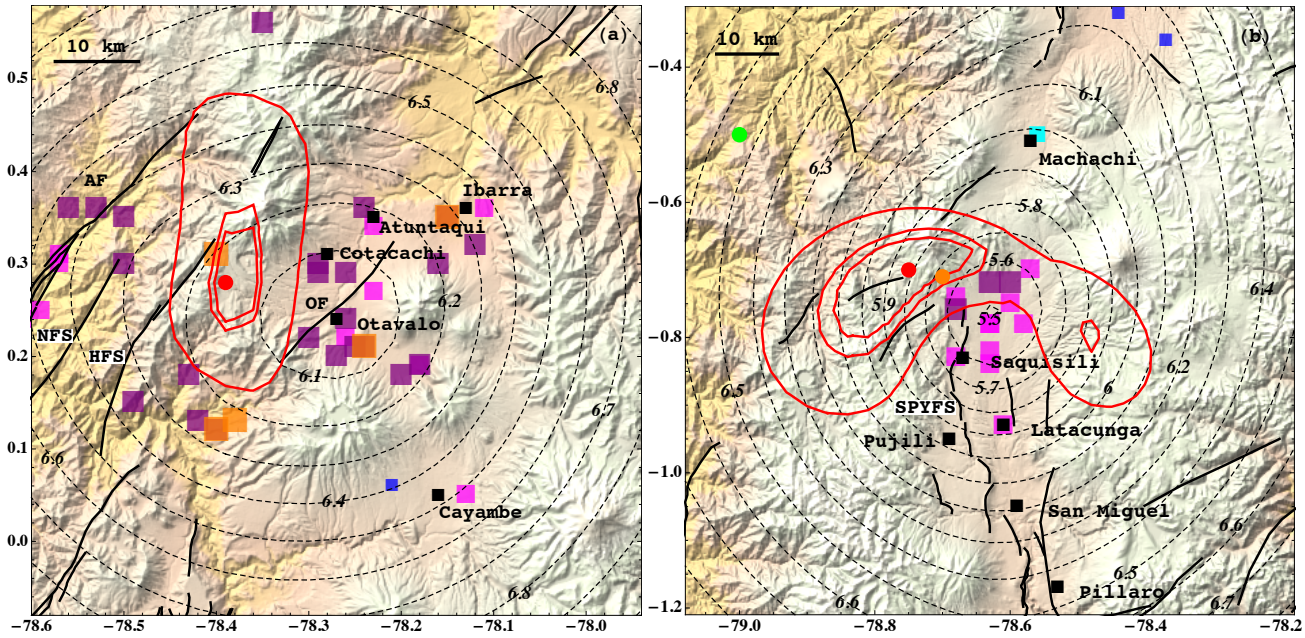


Figure 9: Determination of magnitude and location for historical events. (a) Atahualpa (1955). (b) Toacazo (1944), instrumental epicentre from CGS (certainly bearing at least 30km uncertainty). AF, NFS, HFS, OF, SPYFS are faults (Table 6). See Legend in Figure 3. Results reported in Table 5.

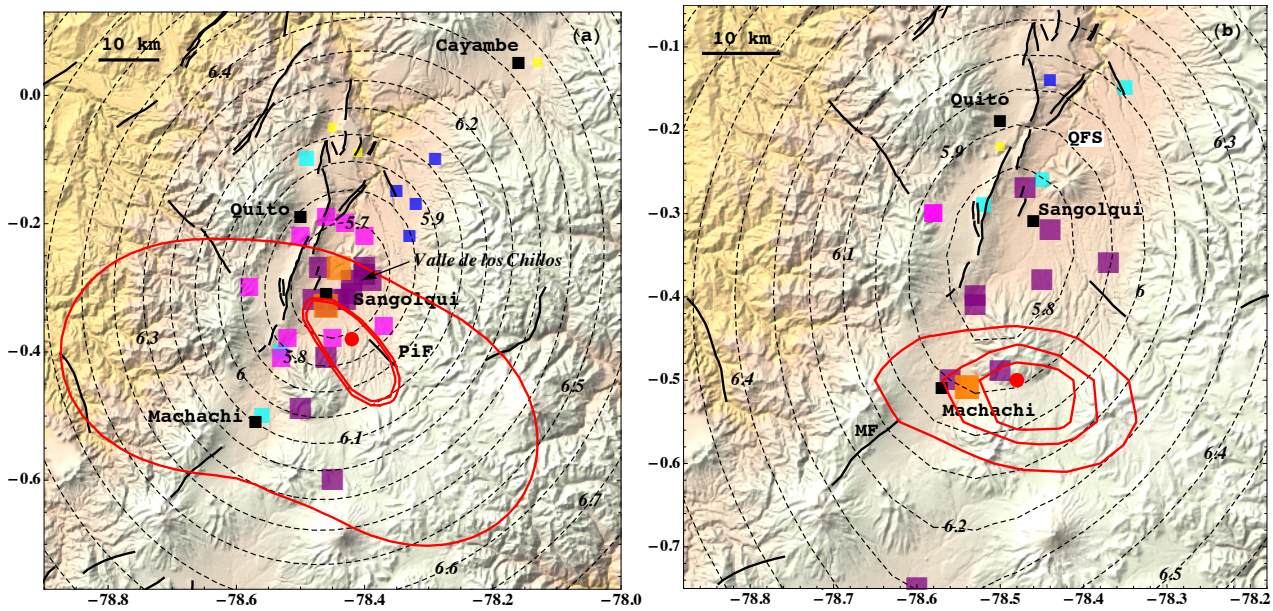


Figure 10: Determination of magnitude and location for historical events. (a) Sangolqui (1938); (b) Murco (1929). PiF and MF are Pintag and Machachi faults (Table 6). See Legend in Figure 3.

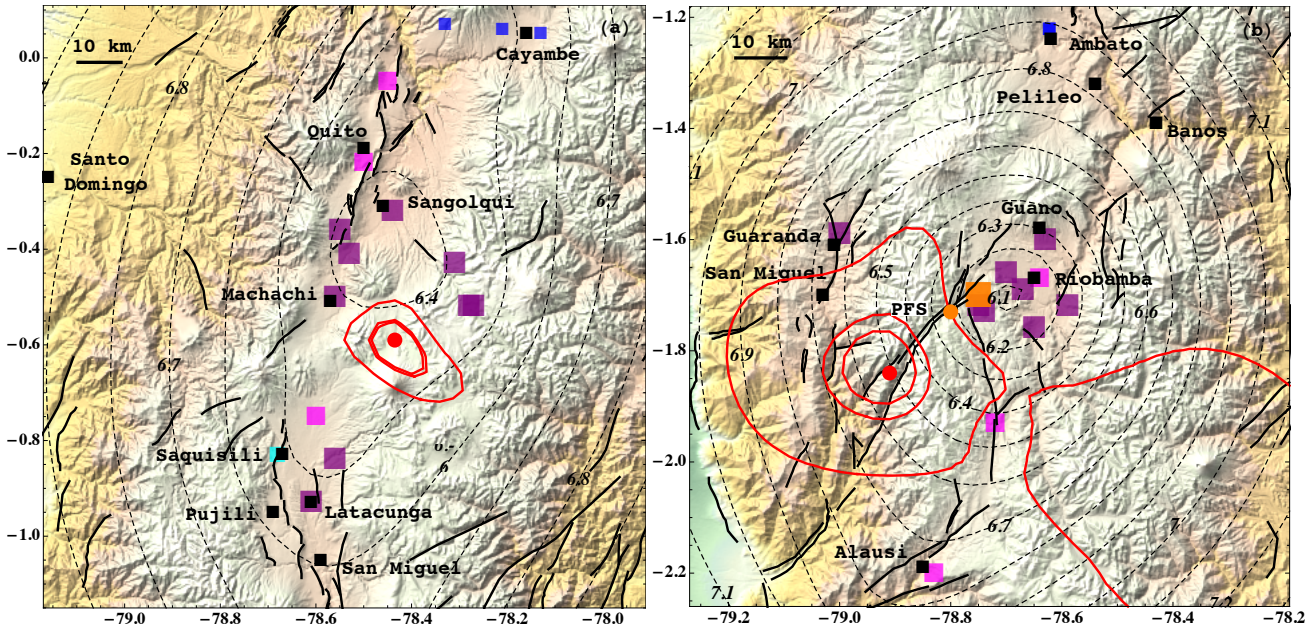


Figure 11: Determination of magnitude and location for historical events. (a) Antisana (1914) based on revised intensities (Singaucho 2009);(b) Cajabamba (1911). PFS is Pallatanga fault system (Table 6). See Legend in Figure 3.

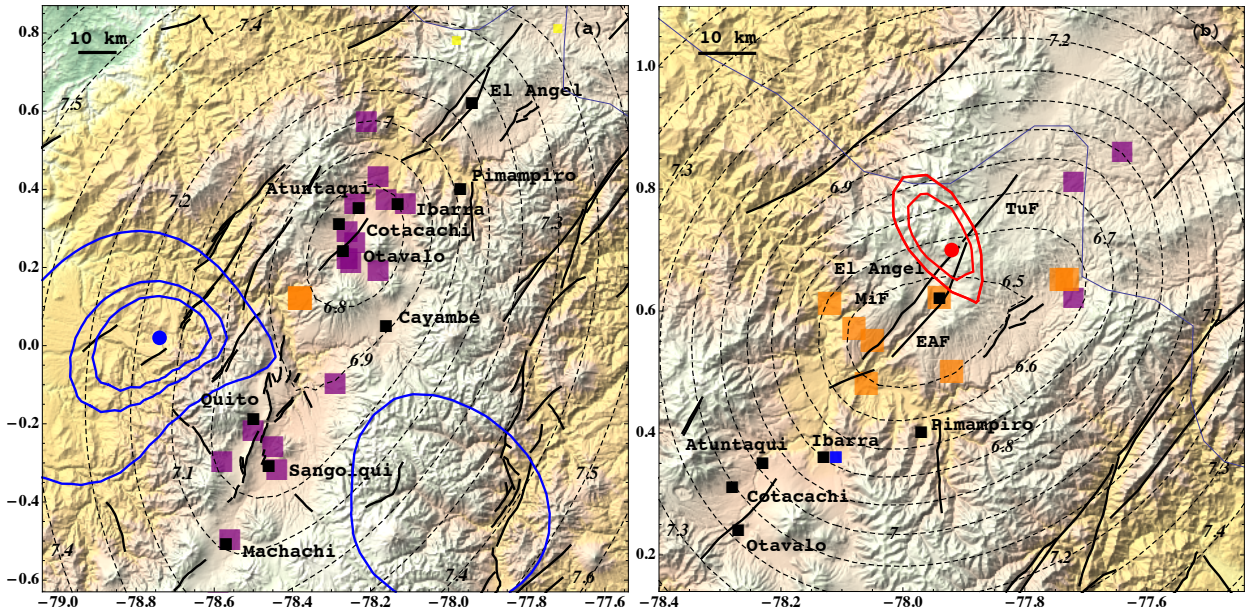


Figure 12: Determination of magnitude and location for historical events. (a) Quito (1859), (b) El Angel (1868). For El Angel, the confidence contour 95% is not drawn, as a very large region would be required. MiF, TuF, EAF are faults (Table 6). See Legend in Figure 3.

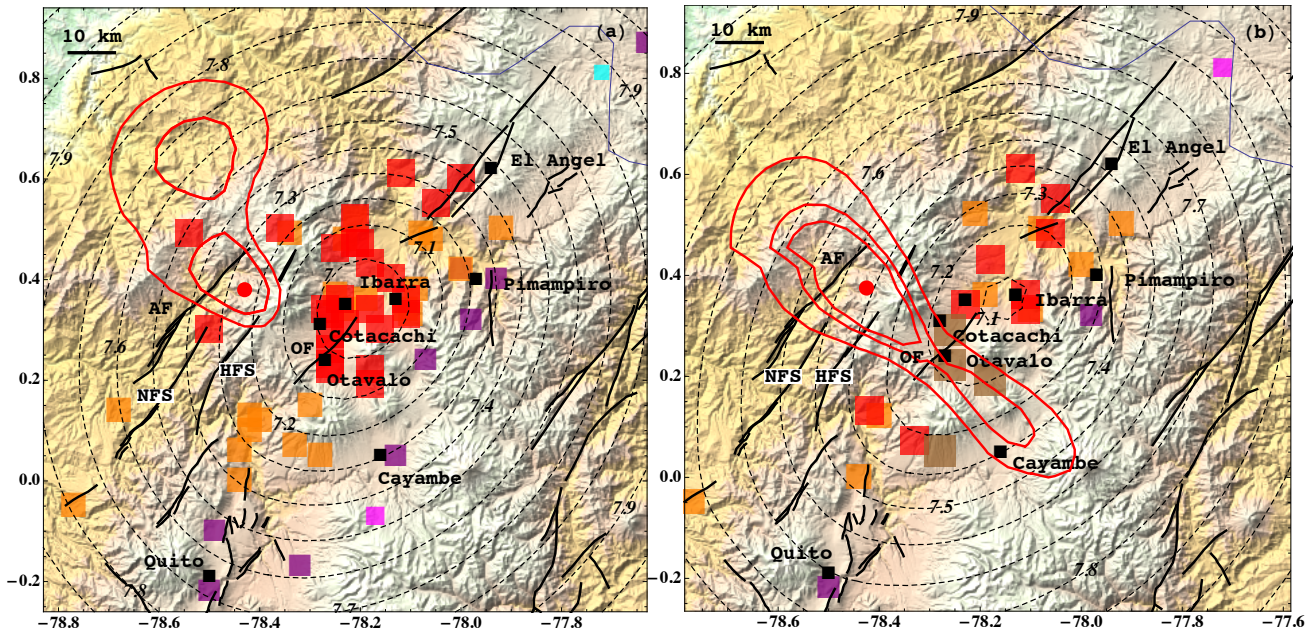


Figure 13: Determination of magnitude and location for Ibarra historical event (1868): (a) original data; (b) revised intensity dataset (Singaucho, 2009). AF, NFS, HFS, OF are faults (Table 6). See Legend in Figure 3.

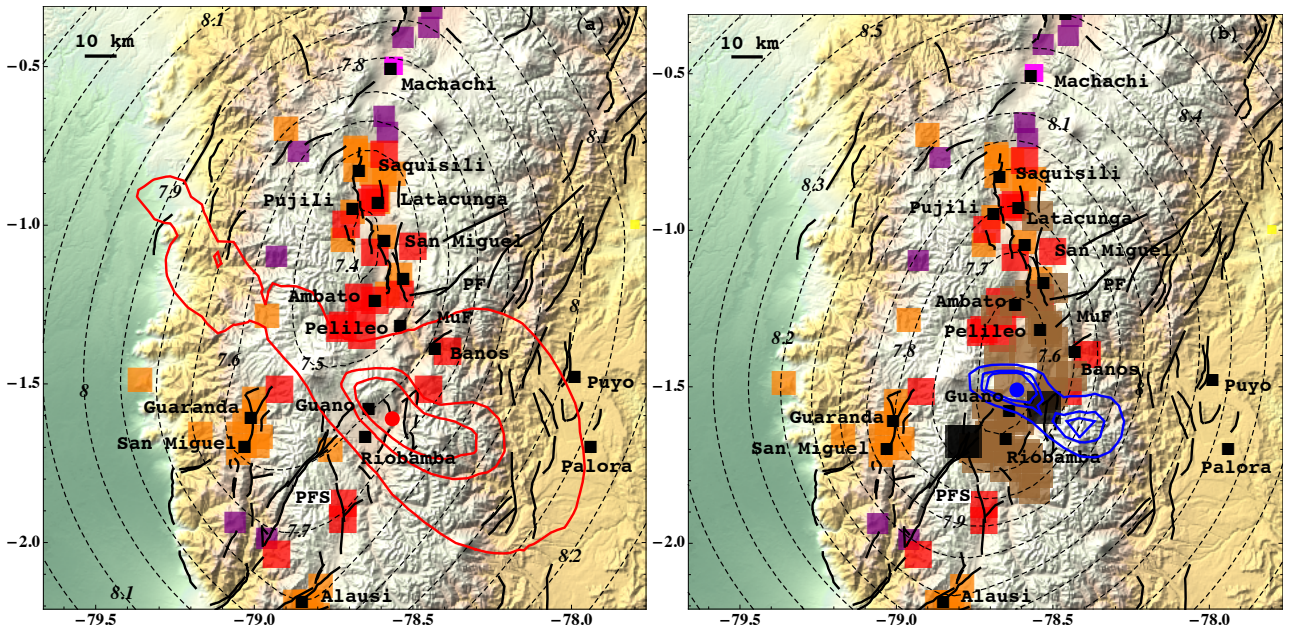


Figure 14: Determination of magnitude and location for Riobamba historical event (1797): (a) using intensities up to IX; (b) using intensities up to XI. PFS is Pallatanga fault system, PF is Pucara fault, MuF is Mundug fault (see Table 6). See Legend in Figure 3.

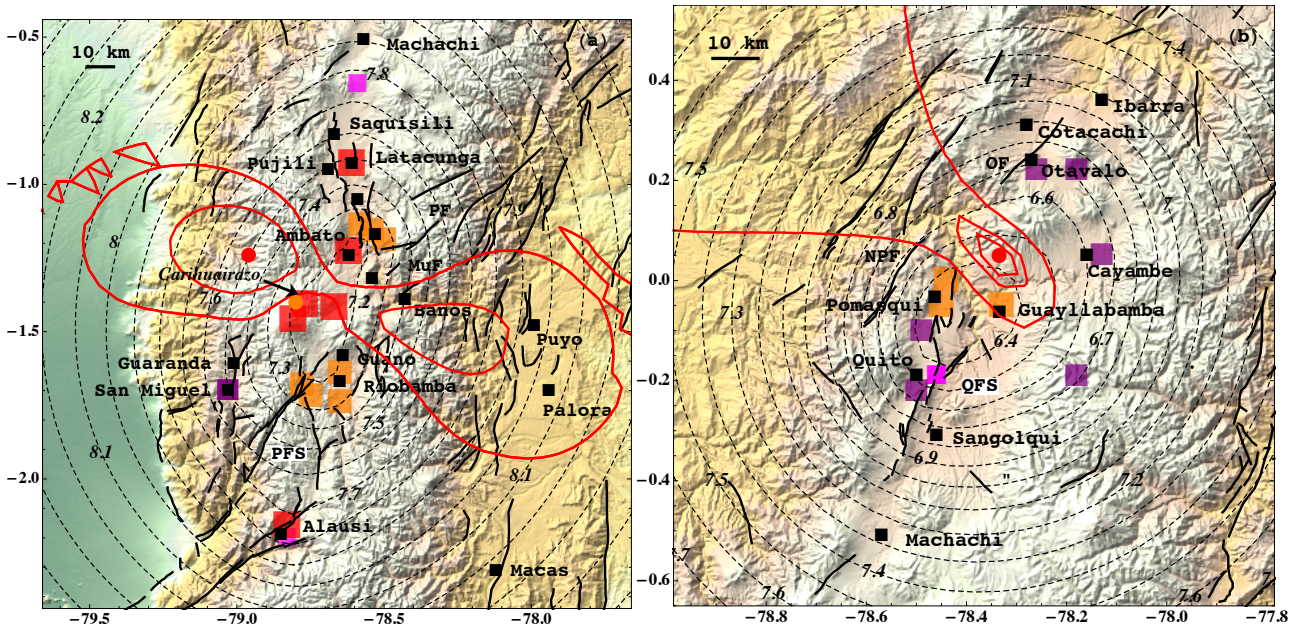


Figure 15: Determination of magnitude and location for (a) the Ambato event (1698): only contours 50 and 67% are drawn, and for the (b) Guayllabamba event (1587). QFS is Quito fault system; NPF is Nono-Pululahua fault (see Table 6). The Carihuairazo is a volcano (see the text). See Legend in Figure 3.

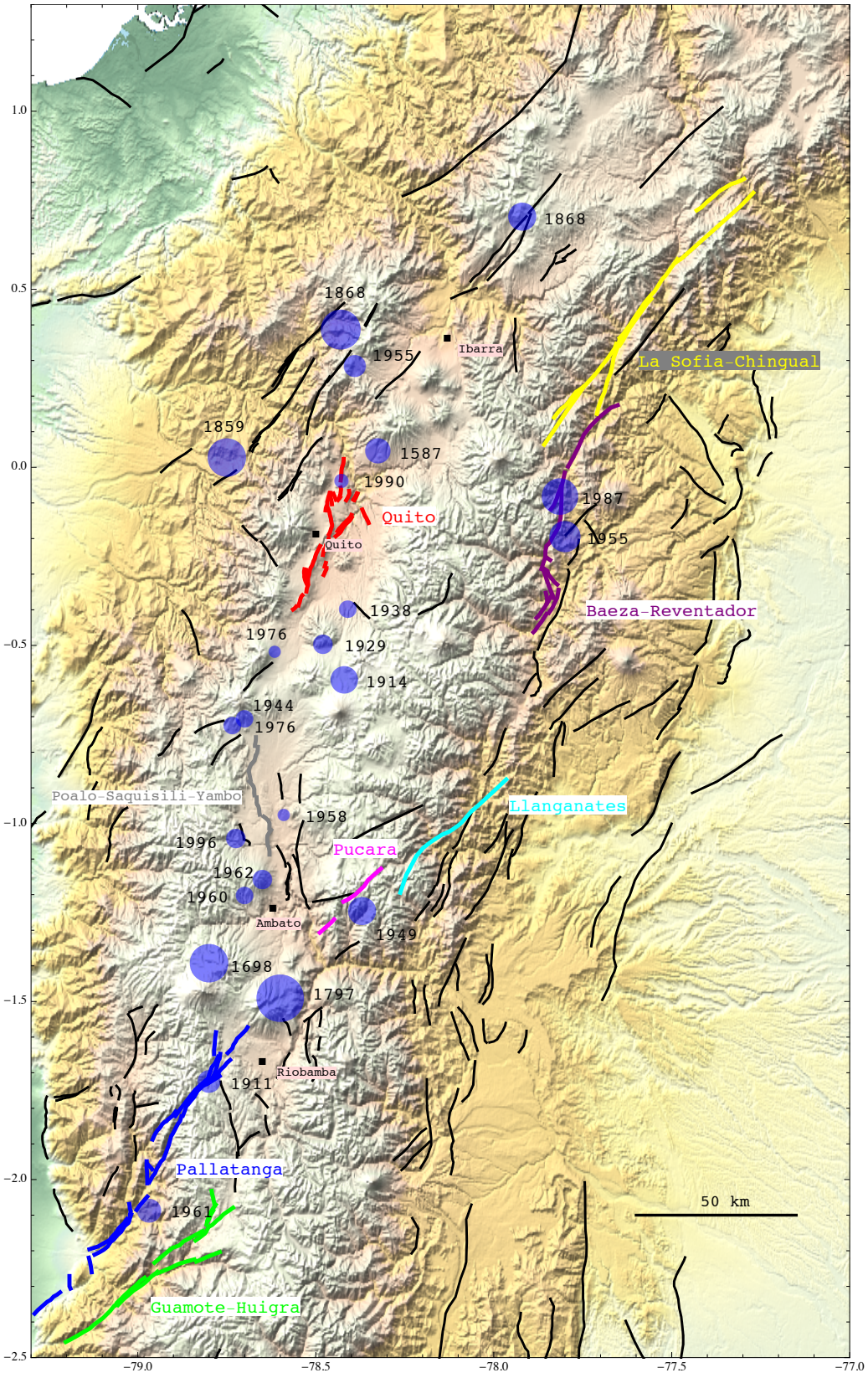


Figure 16: All events studied in the paper, located either in the Interandean Valley either within the Cordilleras. The larger the magnitude, the larger the radius of the blue disk (see values in Tables 3 & 5). The earthquake's year is indicated on the right of each disk. Black thick lines: fault segments (Alvarado, 2009). Specific fault systems highlighted (see text).